UNIVERSITÁ POLITECNICA DELLE MARCHE

FACULTY OF ENGINEERING

Course of Biomedical Engineering

GUI-oriented analysis of posture, gait and EMG

Didactic project of Bioengineering of Motor Rehabilitation

Luca Buscarini, Lucia Migliorelli, Luca A. Pettinari

A.A 2017/2018

Introduction

Rehabilitation Engineering is the application of science and technology to improve the quality of life for people with disabilities [1]. In particular, in the scope of Biomechanics, the main purpose is to tease out information about the functioning of the skeletal, muscular and somatic nervous system, and to determine by the use of objective, reliable and repeatable tests an evaluation of possible dysfunctions affecting an individual. A pivoting point of rehabilitation engineering is functional evaluation, defined in most generic way as a set of tests, protocols, practices and observations that are combined to determine the ability of the evaluated patient to correctly function in one or more tasks. In this scope, functional evaluation addresses the issues related to the assessment of motor function in the presence of disability, and its goal is the development of tools and methodologies that are tailored for the analysis of motor disability based on quantitative criteria. Essentially, a functional evaluation of the subject can help the clinicians to *i*) Plan or customize rehabilitation program (aid to therapy). *ii*) Confirm or change diagnosis of motor dysfunctions or diseases. *iii*) Verify efficacy of treatments and compare outcomes among cases. The aim of this work is to elaborate, describe and analyze critically a whole data-set of acquisitions obtained by a number of different trials which point to the assessment and quantification of factors entailing a particular functioning of a motor task or pattern. Precisely, all the trials collected during these laboratory experiences were divided in three main groups:

1. Posturagraphy analysis.
2. Gait analysis.
3. Electromyography.

In order to manage adequately the visual rendition and organization of the various outcomes and graphs obtained these three points, we propose a tailored Graphic User Interface (GUI), to either facilitate the user experience in the use of the processing software developed in line with the ongoing protocols and conventions, or analyze and compare outcomes from the many acquisitions and data yielded from laboratory trials. At the start, the graphic interface (which from now on said `SimpleGUI`) showcase the following screen in 1.
The buttons on the left side retrace the laboratory experiences, plus a quit button to exit the program. All the features related to these three options will be discussed further in the related

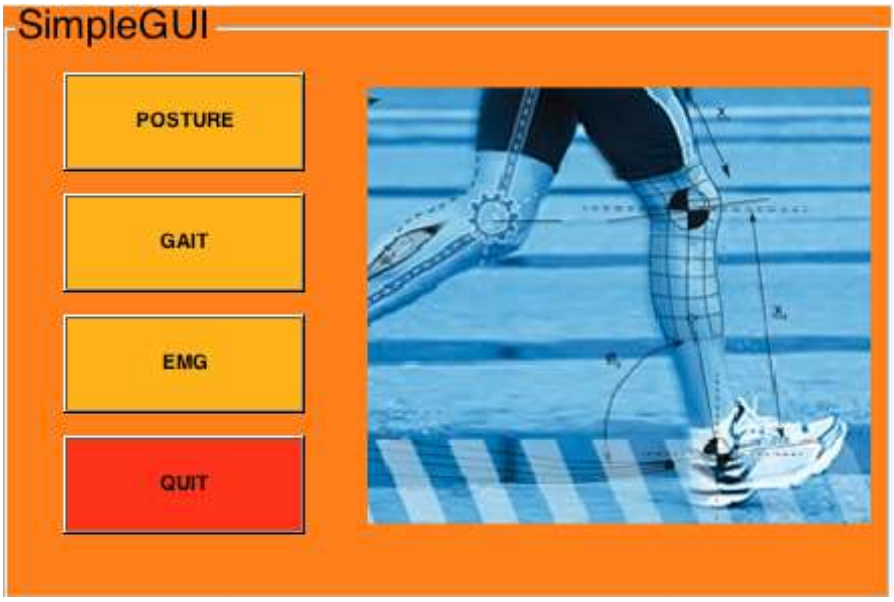

Figure 1: Start menú of `SimpleGUI`

sections. The programming approach here is an object-oriented paradigm (OOP) and the code has been written using the MATLAB platform, which made available a extremely high-level and usable syntax, easily affordable also by non expert programmers [2]. To be noted, the use of objects is not limited only for UI elements, but somewhat encompasses almost the whole code-writing, basically for three reasons:

- Software objects are the abstract projections of real-world things, capturing their attributes (properties of the object) and related concepts (methods of the object).
- Code is organized in classes (abstraction of "world's categories" - objects are instances of classes), favouring the re-use of code and the creation of new classes (hierarchy of classes) starting from the already defined one.
- OOP allows a easy management of big-dimension projects, due to the high modularity of objects as functional boxes.

Posturography

The fact that we as humans are bipeds and locomote over the ground with one foot in contact (walking), no feet in contact (running), or both feet in contact (standing) creates a major challenge to our balance control system. In fact, the presence of a control is necessary since the two thirds of body mass is concentrated up to two thirds of the body height, making the human stance an intrinsic unstable state of our locomotor system. Postural steadiness is the dynamics of the postural control system associated with maintaining balance during quiet standing [3]. The control of posture is maintained by a complex sensorimotor system, which integrates information from the visual, vestibular, and somatosensory system. Measures of postural steadiness are used to characterize the dynamics of postural control system associated with maintaining balance during quiet standing. In our experience, we have studied static and dynamic posturography, principally characterizing the many trials executed with stabilograms, statokinesigrams and Prieto parameters.

Materials

The experiment was conducted in the laboratory of movement analysis of UNIVPM, and data acquisition was carried out by laboratory experts. The main acquisition systems used were:

- A ELITEClinic-BTSEngineering stereophotgrammy system made of 6 TVC cameras (figures 2, 3) to acquire markers position in a global reference system (laboratory frame); sampling frequency $f_c = 100Hz$.
- Placed along a walkway of $11,5m$ of length, a couple of Bertec force platforms, based on extensimetric (GR1) and piezoelectric (GR3) measures, with dimensions $0.4m \times 0.6m$ either (see fig. 4) to acquire dynamic datas like forces and moments, expressed in their solidal reference frame; sampling frequency $f_c = 500Hz$.
- A Wii Balance Board by Nintendo, used to acquire COP position in postural and functional reach trials as an alternative of extensimetric ground reaction platforms; its acquisition method relies on dynamic sampling.

Figure 2: A TVC camera, frontal view.

Figure 3: Side details.

In this particular section, the force platforms were used to estimate the COP (centre of pressure) displacement, while cameras were used to track the subject's feet position among various trials. The COP-based measures were taken on 2 healthy young adults, one male and one female of 24 years. The laboratory frame was fix using a rigid wand with markers located on the center of GR3. Therefore, there were performed different posture assessment trials in the following order, repeated for both subjects:

1. Vertical stance with open eyes (OE) and both feet in one platform (GR1).
2. Vertical stance with closed eyes (CE) and both feet in one platform (GR1).
3. Vertical stance with open eyes (OE), with right foot on GR1 platform and left foot on GR3 platform.
4. Vertical stance with closed eyes (CE) with right foot on GR1 platform and left foot on GR3 platform.
5. Gait initiation test starting with right foot and using both GR1 and GR3.
6. Vertical stance with open eyes (OE) on Wii balance board and GR1 simultaneously on.
7. Functional reach test (FR) on Wii balance board and GR1 simultaneously on.

Figure 4: Ground Reaction Platform 1 and 3.

Methods

Postural steadiness is characterized with measure based on the displacement of the center of pressure (COP), the horizontal and the vertical reaction force that is measured in laboratory with a force platform. The COP is the point location of the vertical ground reaction force vector on the surface of the platform on which the subject stands, and is attained by weighted average of every stress field vectors established in the plate when feet are in contact. Its projections about forward and lateral direction with respect to the vanishing point are said anterior-posterior (AP) and the medial-lateral (ML) component of the COP, and are directly provided by the platform. In this section, we can divide methods in two main groups: those extracted by [3] in order to obtain useful parameters for the postural assessment and comparison and those used to adjust or improve the final representation of the outcomes. Starting from the first, considering the time-series $AP[n]$ and $ML[n]$, it is possible to give an evaluation to the postural steadiness by a plethora of indexes calculated upon, known as Prieto's parameters. The preliminary step was a low-pass filtering with a cut-off frequency $f_c = 5Hz$; the chosen filter is a fourth order FIR Butterworth filter, designed to have a zero-phase shift in order to avoid delays in frequency components. Moreover, of the acquired data only the last $20s$ are considered. Then, the filtered time-series are linearly detrendend (detrendend time-series will be known as AP_0 and ML_0), and can be finally used to implement all the procedures and formula stated by [3]. To begin with, the COP was obtained by AP and ML coordinates, more precisely by AP_0 and ML_0 that are the time-series relative to the origins of the force platform coordinates system. These two components were filtered through fourth-order zero phase Butter-worth low-pass digital filter with a 5Hz cut-off frequency and were taken only the last $20s$ (from the $30s$) for the study. After the definition of the mean COP, that is the arithmetic means of the AP_0 and ML_0 time series so the position on the force platform, all the Prieto's parameters were evaluated. The AP and ML averages are calculated as:

$$\overline{AP} = \frac{1}{N}\sum_{n=1}^{N} AP_0[n] \tag{1}$$

$$\overline{ML} = \frac{1}{N}\sum_{n=1}^{N} ML_0[n] \tag{2}$$

where N is the number of samples. Then, the detrended versions are:

$$AP[n] = AP_0 - \overline{AP} \tag{3}$$

$$ML[n] = ML_0 - \overline{ML} \tag{4}$$

The COP coordinate time-series, AP and ML, are commonly used to compute measures of postural steadiness, and characterize the static performance of the postural control system. In the strict sense, these axes are referenced to the force platform, not the subject. To evaluate the

postural control system in a natural state, the subjects are allowed to stand in a comfortable self-chosen stance, facing toward the positive AP direction of the force platform. Since the orientation of the support base is only approximately aligned with the axes of the force platform, measures based on the AP time series probably reflect some ML movements of the subject, and vice versa. Postural steadiness measures are also computed with another time series, which is derived from the COP but is not sensitive to the orientation of the base-of-support with respect to the force platform. The resultant distance (RD) time series is the vector distance from the mean COP to each pair of points in the AP_0 and ML_0 time series.

$$RD[n] = \sqrt{AP[n]^2 + ML[n]^2} \tag{5}$$

Starting from these sets of data, the effective Prieto parameters were computed, dividing them along three main belonging categories:

1. **Time-domain distance measures**.

   - MDIST (average resultant distance). Average distance from COP, computed as the mean of the resultant distance (RD) timeseries:

   $$MDIST = \frac{1}{N}\sum_{n=1}^{N} RD[n] \tag{6}$$

   - RDIST (root mean square distance). The distance from the mean COP, is the root mean square value of the RD time series:

   $$RDIST = \sqrt{\frac{1}{N}\sum_{n=1}^{N} RD[n]^2} \tag{7}$$

   - TOTEX (total excursion). It is the total length of the COP path:

   $$TOTEX = \sum_{n=1}^{N-1} (AP[n+1] - AP[n])^2 + (ML[n+1] - ML[n])^2 \tag{8}$$

   - MVELO (mean velocity). It is the average velocity of the COP:

   $$MVELO = \frac{TOTEX}{T} \tag{9}$$

     where T is the total time interval during while data are acquired.

2. **Time-domain area measures**.

   - AREA-CC (95% confidence-circle area). It is the area of a circle with the area equal

to the one-sided 95% confidence limit of the RD time series;

$$AREA_{CC} = \pi(MDIST + z_{0.5}s_{RD})^2 \tag{10}$$

with s_{RD} the root mean square of RD, and $z_{0.5}$ is the z statistic at the 95 % ($z_{0.5} = 1.645$).

- AREA-CE (95% confidence ellipse area) It is the area of the 95% bivariate confidence ellipse:

$$AREA_{CE} = \pi ab \tag{11}$$

The quantities a and b are respectively the minor and major semi-axes of the ellipse:

$$a = \sqrt{F_{\cdot 05[2,n-2]}(s_{AP}^2 + s_{ML}^2 + D)} \tag{12}$$

$$b = \sqrt{F_{\cdot 05[2,n-2]}(s_{AP}^2 + s_{ML}^2 - D)} \tag{13}$$

where $F_{\cdot 05[2,n-2]}$ is the F statistic at a 95% confidence level for a bivariate distribution with n data points. The quantity indicated with D equals to:

$$D = \sqrt{(s_{AP}^2 + s_{ML}^2) - 4(s_{AP}s_{ML} - s_{APML}^2)} \tag{14}$$

where s_{APML} is the covariance between $AP[n]$ and $ML[n]$:

$$s_{APML} = \frac{1}{N}\sum_{n=1}^{N} AP[n]ML[n] \tag{15}$$

3. **Time-Domain hybrid measures**.

- AREA-SW (sway area). It is the area enclosed by the COP path per unit of time, and is calculated:

$$AREA_{SW} = \frac{1}{2T}\sum_{n=1}^{N-1}\Big|AP[n-1]ML[n] - AP[n]ML[n-1]\Big| \tag{16}$$

- MFREQ (mean frequency). It is the rotational frequency, that is an estimate of how much fast the COP trajectory wraps about is center:

$$MFREQ = \frac{TOTEX}{2\pi MDIST \cdot T} = \frac{MVELO}{2\pi MDIST} \tag{17}$$

- MFREQ-AP (mean frequency in anterior-posterior direction). It is the frequency of a sinusoidal oscillation with an average value of mean distance of AP:

$$MFREQ_{AP} = \frac{TOTEX}{4\sqrt{2}MDIST \cdot T} = \frac{MVELO}{4\sqrt{2}MDIST} \tag{18}$$

4. **Frequency-Domain measures**.

   - SPECTRAL MOMENTS. Defined as:

$$\mu_k = \sum_{m=i}^{j} (m\Delta f)^k G[m] \tag{19}$$

     G is the generic notation for the spectrum of one of the signals among AP,ML and RD. The zero-order moment (μ_0) coincides with the total power of the signal-

   - 50% POWER FREQUENCY. It is the frequency below which 50% of the total power area is found:

$$\sum_{m=i}^{\mu} G[m] \geqslant 0.50\mu_0 \tag{20}$$

   - 95% POWER FREQUENCY the frequency below which 95% of the total power is found.

$$\sum_{m=i}^{\nu} G[m] \geqslant 0.95\mu_0 \tag{21}$$

These parameters are general indexes for COP displacement. Though, having tested subjects in different type of experiments, it is necessary to furnish the adequate $AP[n]$ and $ML[n]$ time-series (from which descend all the Prieto parameters) in order to obtain the correct results. In general, the major issue is that each acquisition device has its own reference frame; therefore, measurements must be expressed is the same one, in order to be comparable and elaborated. In our case, considering a bird's eye view of the laboratory floor, the main reference frames were disposed as follow:

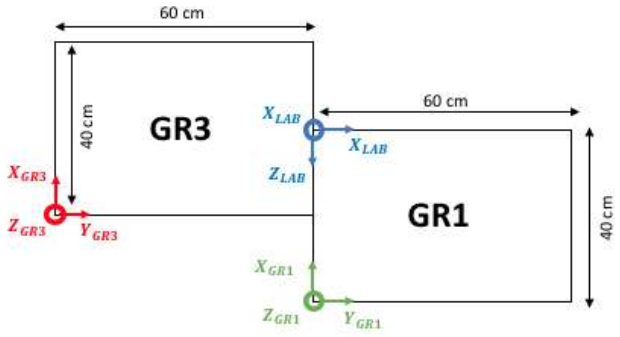

Figure 5: Reference systems in use.

The tern $\{X_{LAB}, Y_{LAB}, Z_{LAB}\}$ is associated with the laboratory system which is considered the global reference frame G (blue one), $\{X_{GR1}, Y_{GR1}, Z_{GR1}\}$ and $\{X_{GR3}, Y_{GR3}, Z_{GR3}\}$ are the local reference systems L_1 (green one) and L_2 (red one) respectively for GR1 and GR3 platforms.

In most generic way, to change the expression of one measurement of position or force from one system to the other ($S_1 \rightarrow S_2$), one must transform all quantity:

$$[\mathbf{m}]_{S_2} = \mathbf{R}^T_{S1/S2}[\mathbf{m}]_{S_1} + [\mathbf{c}]_{S_2} \tag{22}$$

where $\mathbf{m}$ is the generic measured vectorial quantity, $\mathbf{R}_{S1/S2}$ is the change of basis matrix from S_1 to S_2 and $\mathbf{c}$ is the distance between S_1 and S_2. Since we consider only two dimensions (the anterior-posterior and the medio-lateral) and all the reference system versors lies on parallel lines, the general expressed in (28) can be simplified following this rule: for any couple of reference systems, when a measure must be expressed with respect to the other, it must be summed by their relative distance, and its coordinates must be provided with a minus sign for every versor of the new reference that points oppositely respect to the older one. Another point in need of adjustment before the calculation of Prieto's parameters was for those trials with two active force platforms. In this case, the computation of the COP_{net} must take in account the single contribution provided by each single foot:

$$COP_{net}(t) = COP_l(t) \cdot \frac{R_{vl}(t)}{R_{vl}(t) + R_{vr}(t)} + COP_r(t) \cdot \frac{R_{vr}(t)}{R_{vl}(t) + R_{vr}(t)} \tag{23}$$

where COP_l and COP_r are the COP under left and right feet respectively, and R_{vl} and R_{vr} are the vertical reaction forces under left and right feet respectively. Finally, we also provided a representation of one of the Prieto's parameters, the ellipse confidence area at 95% (e.g. the area in which the 95% of the signal is expected to be found). The parameter itself provides the value of the area, but gives no hint about the analytic expression of the ellipse. Being note both major and minor the semi-axes from (12) and (13), a generic ellipse can be expressed in parametric form as:

$$\begin{cases} x(t) = a \cdot \cos(\omega t); \\ y(t) = b \cdot \sin(\omega t); \end{cases} \tag{24}$$

This geometric object must be properly oriented to match the 95% confidence area. This problem is solved by applying to data a statistical signal processing technique known as principal component analysis (PCA). In short, taken the covariance matrix of the data (in this case it is 2×2 matrix), its EVD (eigenvalues decomposition) provides eigenvectors lying on the direction of maximal linear uncorrelation, i.e. the directions in which one principal component is virtually determined without dependency from the other. These directions are orthonormal and can be stuck in a rotation matrix in order to obtain a new orientation of the ellipse, which mirrors the directions of principal components. Once found $\mathbf{R} = [\mathbf{u} \quad \mathbf{v}]$, with $\mathbf{u}$, $\mathbf{v}$ eigenvectors associated with the covariance matrix, the parametric equations of ellipse become:

$$\begin{bmatrix} x'(t) \\ y'(t) \end{bmatrix} = \mathbf{R} \begin{bmatrix} x(t) \\ y(t) \end{bmatrix} \tag{25}$$

The graphic outcome is:

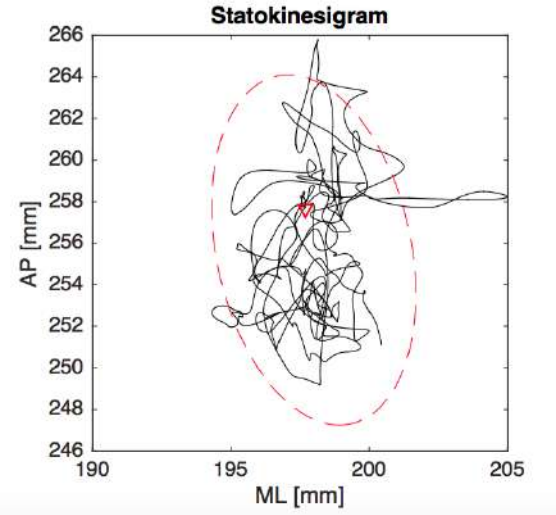

Figure 6: Statokinesigram with ellipse confidence area at 95 %

To be noted, for the NWBB the AP and ML were calculated in the following way:

$$COP_{NWBB,x} = \frac{X}{2}\frac{(F_{TR} + F_{BR}) - (F_{TL} + F_{BL})}{F_{TR} + F_{BR} + F_{TL} + F_{BL}} \tag{26}$$

$$COP_{NWBB,y} = \frac{Y}{2}\frac{(F_{TR} + F_{TL}) - (F_{BR} + F_{BL})}{F_{TR} + F_{BR} + F_{TL} + F_{BL}} \tag{27}$$

where $X = 433mm$ and $Y = 238mm$, F_{TL}, F_{TR}, F_{BL} and F_{BR} are the forces measured by the NWBB platform. The NWBB measures with respect to its own reference system, therefore it will be necessary to apply the same expedient described previously.

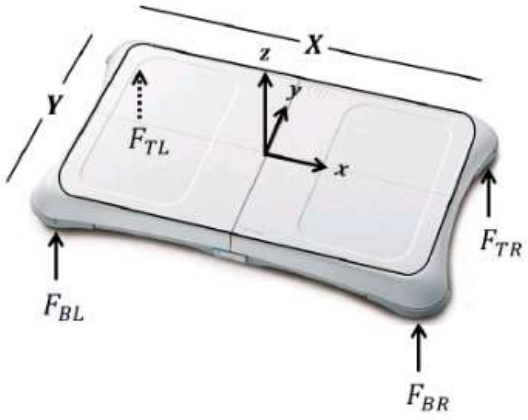

Figure 7: NWBB

Discussion and conclusions

The dialog window showing at the click of the first option of the start menú panel of `SimpleGUI` gives three possible modalities to choose from: `Standard`, `Twoplates` and `Nintendo`. In fact, in this first laboratory experience all trial could be organized in three categories, based on the use of one platform (GR1), two platforms (GR1/GR3) and the Nintendo Wii Balance Board (NWBB). At this point, the user is allowed to analyze four different situations. The possibilities are: stabilograms of both AP and ML directions; statokinesigram, with the feature buttons to show ellipse confidence area, feet location and even platform location; time-evolution statokinesigram, which takes in account time variable, yielding a 3D plot; table with Prieto's parameters. We will continue distinguishing the three categories of experiments done (see description of various trials in the Material section).

- **Standard**.
  Standard mode comprises all the trials in which is involved only one platform; it can be performed both for male and female subjects, with the use of vision (OE - open eyes) or without (CE - closed eyes). The absence of one of the three sensory system alters the action of our balance control system. Using the implementation of the core of [3] (`calculateprieto.m`), Prieto's parameters found for the female subject are organized in 1. Open eyes stabilograms in AP and ML directions have the following trends:

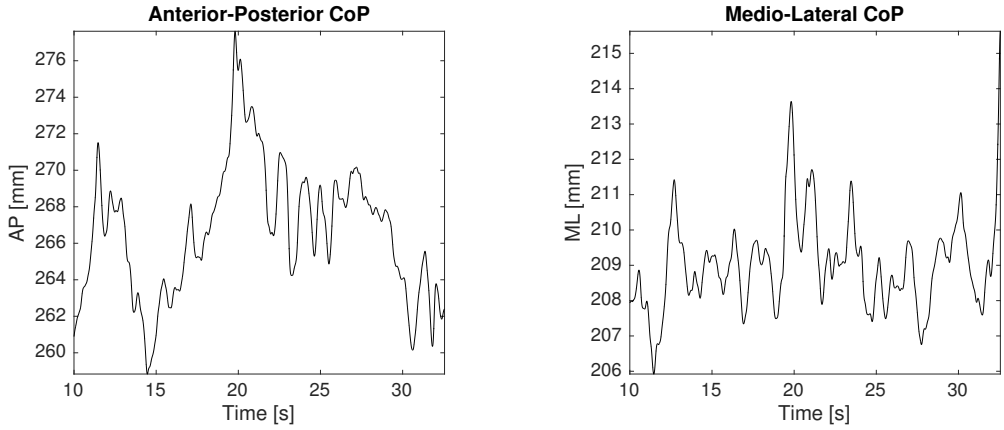

Figure 8: Stabilograms of OE posture trials on a single platform (GR1).

In case of closed eyes, the stabilograms yield:

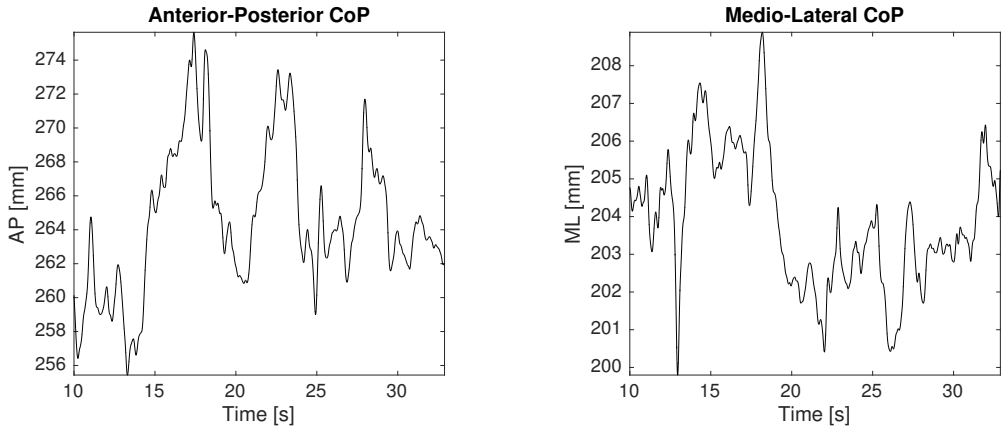

Figure 9: Stabilograms of CE posture trials on a single platform (GR1).

Looking at statokinesigrams, in case of closed eyes the confidence ellipse is bigger than the one in open eyes, meaning a wider displacement of the COP in the first case:

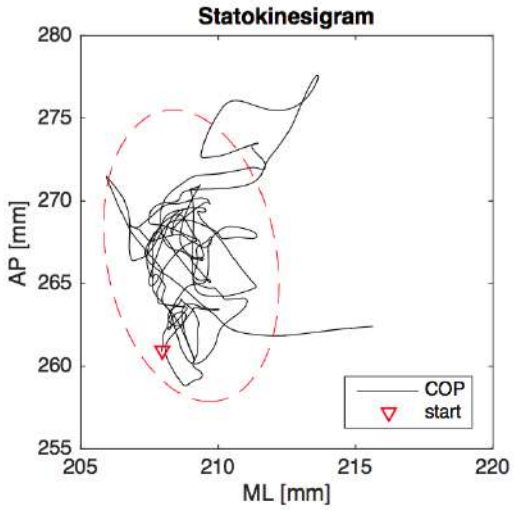

Figure 10: Open eyes statokinesigram.

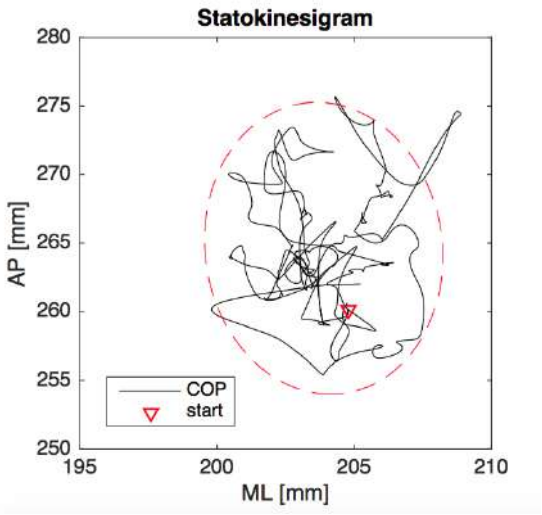

Figure 11: Closed eyes statokinesigram.

For the option of statokinesigram 12, we made also available the possibility of plotting feet, and platform as points of reference. For example, the button *PLATFORM* (which enables only when *FEET* button has been clicked) plot the platform under the feet as in figure 13 :

PARAMETER	OPEN EYES (OE)	CLOSED EYES (CE)	ROMBERG RATIO
$MDIST$	338.8425	334.0686	0.9859
$MDIST\_AP$	266.6820	264.6250	0.9923
$RDIST$	338.8568	334.0888	0.9859
$RDIST\_AP$	266.7063	264.6607	0.9923
$MVELO$	8.0538	9.5411	1.1847
$MVELO\_AP$	6.3231	7.9096	1.2509
$AREA\_CC$	371660	363410	0.9778
$AREA\_SW$	821.1535	953.5484	1.1612
$MFREQ$	0.0038	0.0045	1.1842
$MFREQ\_AP$	0.0042	0.0053	1.3947
μ_0_AP	71132	70045	0.98471
μ_0_ML	43692	41570	0.9514
μ_0_RD	114820	111620	0.9721
f_50_AP	0.27	0.27	1
f_50_ML	0.46	0.38	0.8261
f_50_RD	0.27	0.27	1
f_90_AP	1.16	1.28	1.1034
f_90_ML	1.38	1.21	0.8768
f_90_MR	1.15	1.32	1.1478

Table 1: Prieto's parameters for subject with open eyes, close eyes and the Romberg ratio

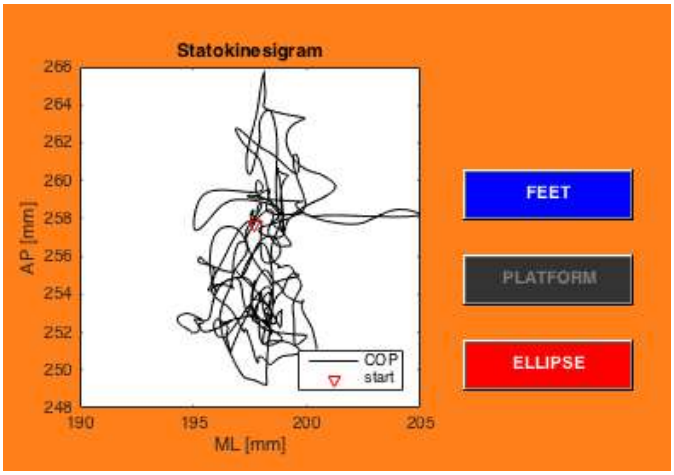

Figure 12: Statokinesigram options.

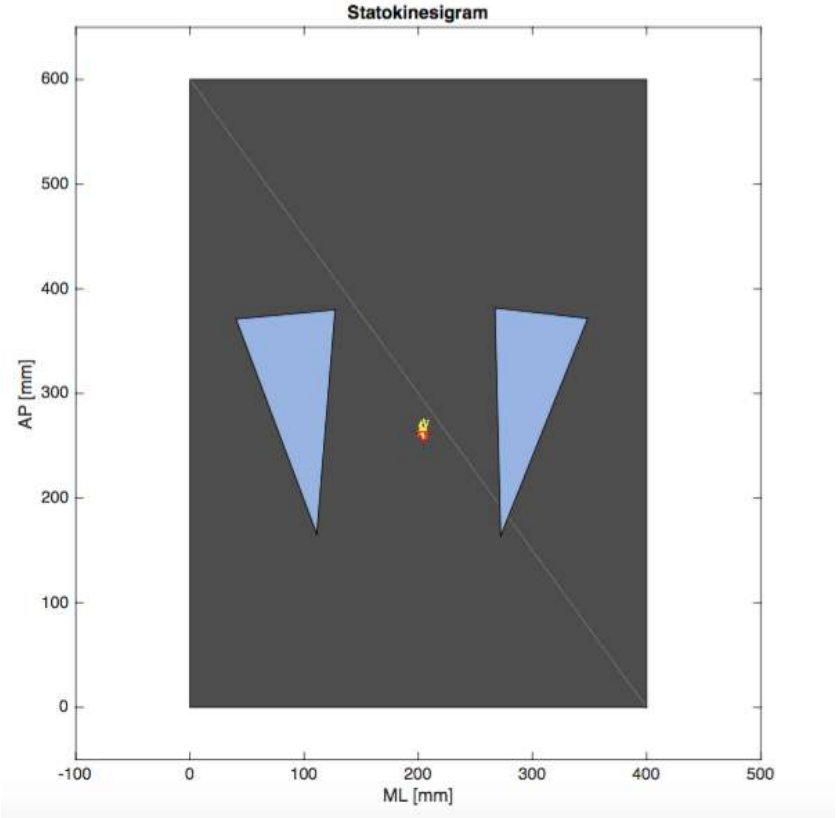

Figure 13: *PLATFORM* option.

PARAMETER	OPEN EYES (OE)	CLOSED EYES (CE)	ROMBERG RATIO
$MDIST$	288.7394	273.9439	0.9488
$MDIST\_AP$	288.5953	273.7677	0.9486
$RDIST$	288.8232	273.9809	0.9486
$RDIST\_AP$	288.6818	273.8060	0.9485
$MVELO$	11.4405	10.9278	0.9552
$MVELO\_AP$	7.9995	7.4480	0.9312
$AREA\_CC$	283090	248690	0.8785
$AREA\_SW$	918.8480	868.8079	0.9455
$MFREQ$	0.0063	0.0063	1
$MFREQ\_AP$	0.0049	0.0048	0.9796
μ_0_AP	83337	74970	0.8996
μ_0_ML	81.6456	95.8230	1.1736
μ_0_RD	83419	75066	0.8999
f_50_AP	0.27	0.31	1.1481
f_50_ML	0.32	0.32	1
f_50_RD	0.23	0.23	1
f_90_AP	0.81	0.81	1
f_90_ML	0.83	0.85	1.0241
f_90_MR	0.77	0.92	1.1948

Table 2: Prieto's parameters for subject with open eyes, close eyes and the Romberg ratio in vertical stance posturography with GR1/GR3 platforms.

The value of Romberg Ratio is almost always lower than one, identifying a better stability during eyes closed.

- **Twoplates**.
  This modality comprises all the trials involving two platforms: in our case, a vertical stance posturography with feet both on active GR1 and GR3, and gait initiation test. For the first case the Prieto's parameters are shown in table 2. Stabilograms are plotted for both AP and ML directions (only for OE trial), overlapping in each components the COP_l, COP_r, and COP_{net},as shown in figure 14. While for the AP direction COP_l and COP_r have almost the same contribution, for the ML it is appreciable a difference in amplitude: this due to the fact that in the balancing action, the loading/unloading mechanism concurs in controlling the COP_net. As in the previous case, feet and platform are featured as GUI user buttons (see figure 15).

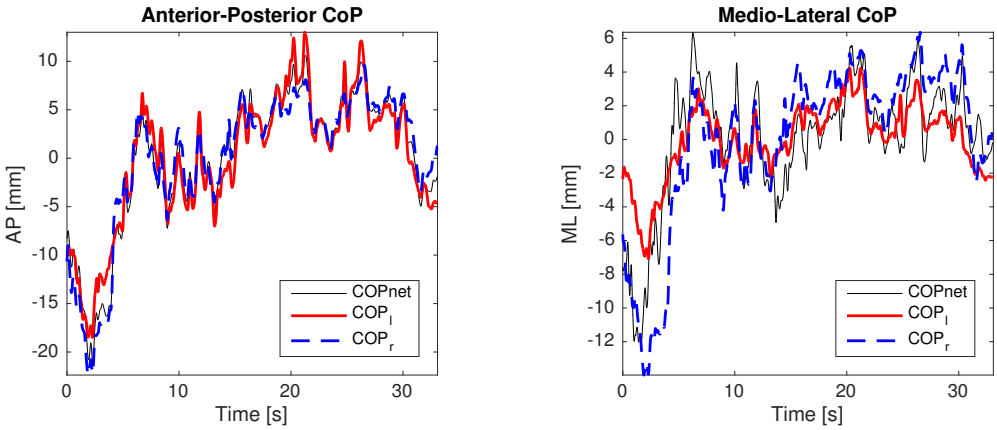

Figure 14: COP_l, COP_r, and COP_{net} compared.

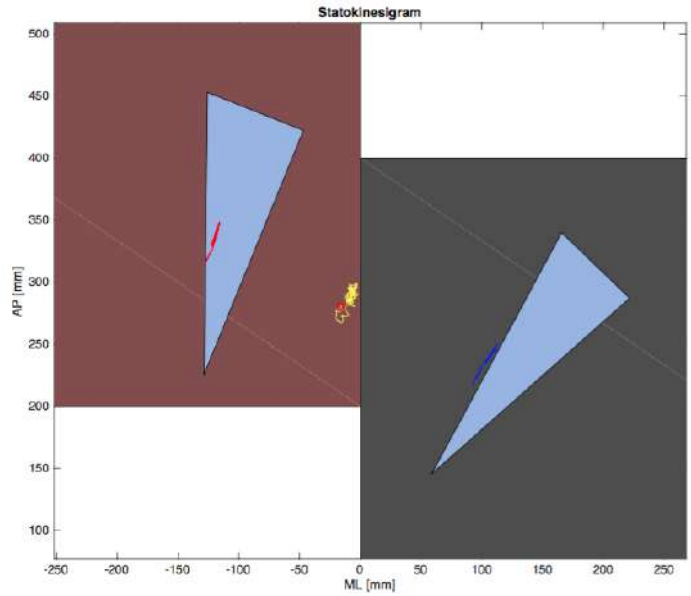

Figure 15: COP_l in red, COP_r in blue, COP_{net} in yellow.

It can be observed that both COP_l and COP_r fall inside the foot, while the COP_{net} fall quite in middle, almost on the border of contact between the two platforms. Also trials of gait initiation test (GI) were performed: the subject had to start swinging the right foot and starting from GR3 towards GR1. For the female subject, the trial yielded the following stabilograms and statokinesigram:

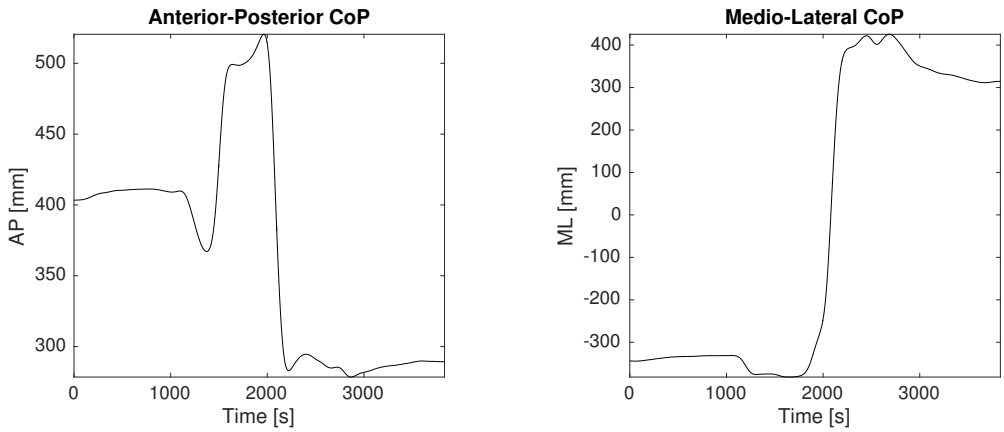

Figure 16: AP and ML directions for gait initiation test.

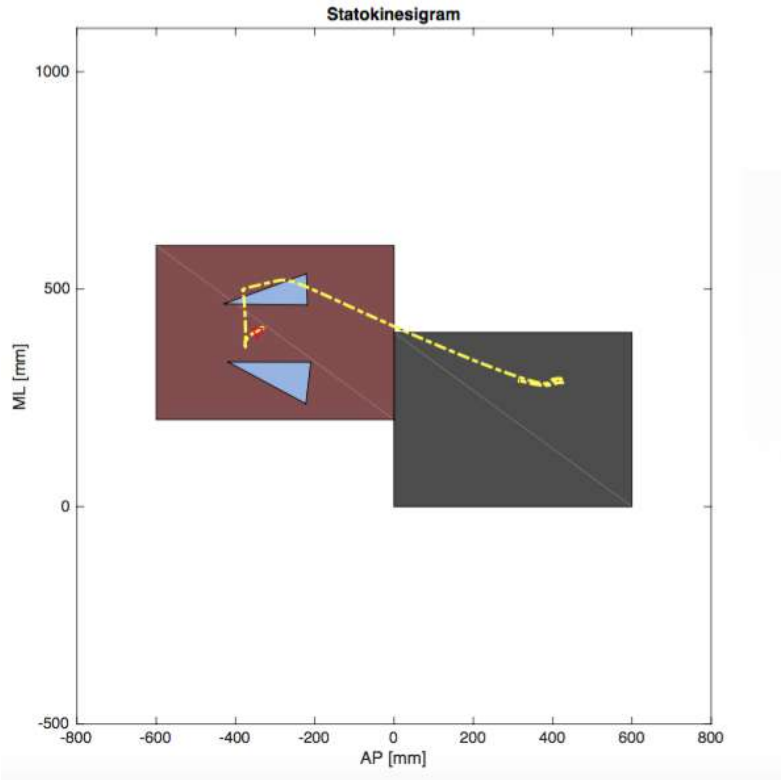

Figure 17: Gait initiation

For what concerns gait initiation, there are all the phases ($S_1 - S_3$): the COP moves behind the COM generating the net moment necessary to move ($S1$,18), then it moves to the opposite foot (unload phase S_2,18),then the COP excurses forward due to an increase of plantarflexors activity on the stance limb (S_3,18).

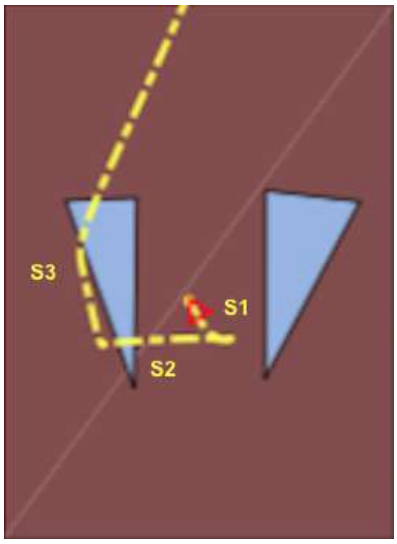

Figure 18: Enlargement of figure 18

- **Nintendo**.

For the NWBB posture trial for the female subject, the stabilograms are:

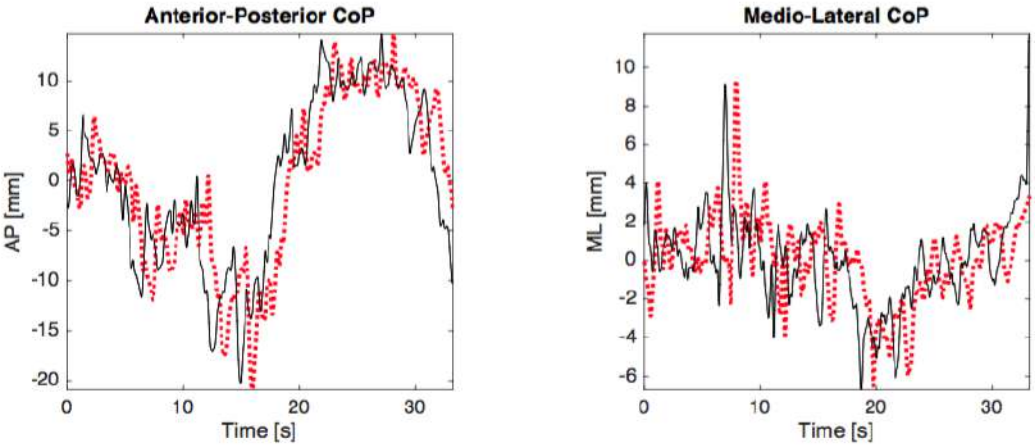

Figure 19: Detail on the delay offered by the NWBB with respect to GR1.

In figure 19, it is appreciable the delay of the platform GR1 data with respect to WII ones. This delay is encoded by the resampling of WII timeseries, which are acquired with a dynamic sampling; to deal with it, we have found a frequency estimate of the non-linearly sampled data, then applied a resampling at $500Hz$ (the f_c sampling frequency of the platforms). The statokinesigram for posture trial with feet and platform is:

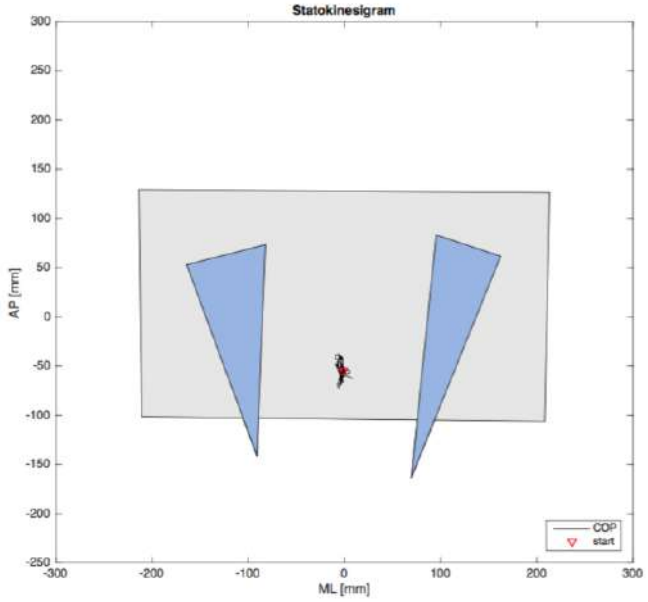

Figure 20: Statokinesigram for posture on NWBB with feet.

Yet, the functional reach test (FR) for the female subject yield the following stabilograms:

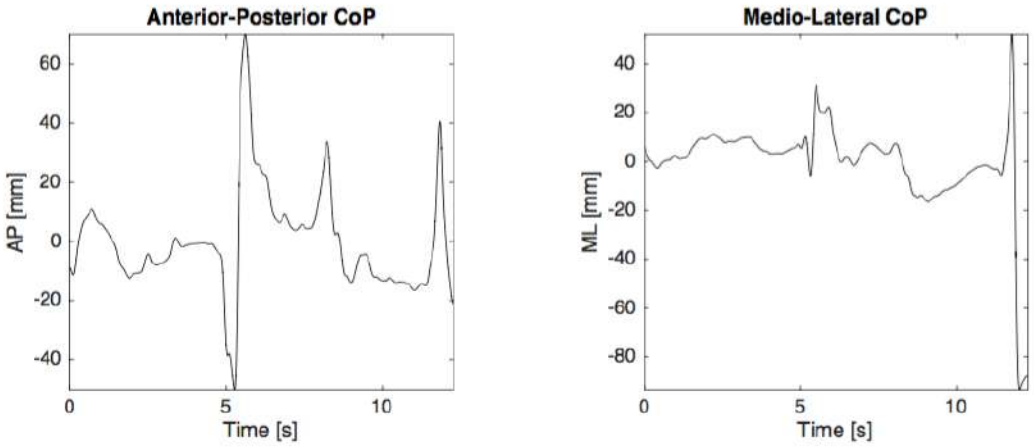

Figure 21: Stabilograms for functional reach test.

In figure 22, the functional reach statokinesigram is:

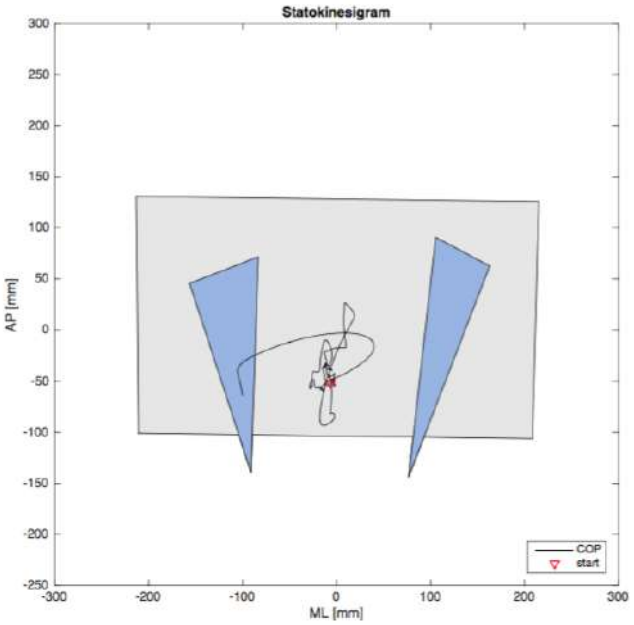

Figure 22: Statokinesigram for functional reach on NWBB.

It is possible to see a moving behind the COG of create the moment to swing the body forward, then moves forward as the load is shifted to the forefoot.

Gait Analysis

Gait analysis is the systemic measurement, description and assessment of those quantities thought to characterize human locomotion [5]. Gait cycle is defined as the period between any two nominally identical events in the gait process. Generally, these two nominally identical events correspond to the instant where one foot strikes the ground and ends when the same foot strikes again the ground (this phase is called initial contact or IC). During the gait cycle, lower limb considered an alternate stance phase (foot in contact with the ground) and swing phase (foot without ground contact). A gait cycle is thus divided in a period of stance phase (about 60% of the cycle) and in a period of swing phase (about 40% of the cycle) of the lower limbs, right and left 23.

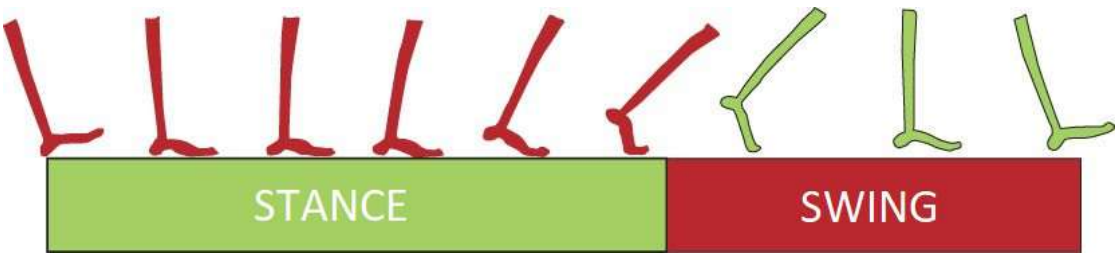

Figure 23: Stride phases

It is possible to make a sub-division according to the stance and swing phase of the two lower limbs. When both members are in stance phase, this is said double support and when one of the two members is in stance phase while the other is in swing phase, this is a single support. More specifically, the stance phase can be divided into five functional sub-phases 25 occurring in the following sequences:

- initial contact (IC);
- loading response (LR);
- mid-stance (MSt);
- terminal stance (TSt);

- pre-swing (PSw).

As the same way, the stance phase is divided into three functional sub-phases occurring in the following sequences:

- initial swing (ISw);
- mid-swing (MSw);
- terminal swing (TSw).

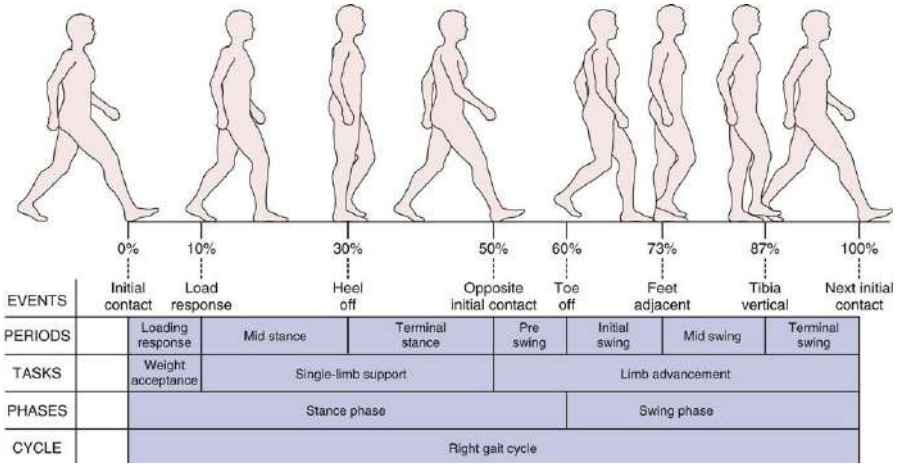

Figure 24: Subdivision of gait cycle

However, we prefer to keep a division according the events occurring during the gait cycle (i.e. first double support, single support, second double support, and swing phase) that permits a more precise definition of the sub-phases and avoids confusion in the terms.
During gait important movement occur in all three planes, sagittal, frontal and transverse. In our experiment we will concentrate the study only on the sagittal plane because here largest movements occur.

Materials

The experiment was conducted in the laboratory of movement analysis of UNIVPM and the data was acquired from one female subject of 24 years, performing a walk with gait developed to speed when passing on the sensing force platforms, which by the way in this case covered a minor role since the aim was to describe gait kinematics by studying her joint angles. For this reason, the main acquisition system for our purpose was, as for the previous experiment, the ELITEClinic-BTSEngineering (6 TVC cameras). Data was sampled at at a sampling frequency of $fc = 100Hz$, and preprocessed with a four-order, zero-shift phase FIR Butterworth filter. Moreover, since the

TVC system assigns a bias value of -9999 if the marker was not seen by at least three cameras, we have implement three procedures to avoid it. In particular: `preparemat.m` ensures that the first and last sample of a given dataseries is different from the bias value, eventually replacing them with first valuable samples. Then the result is passed to `cleanmat.m` which provides an interpolated signal with the same number of sample of the biased one, calling in its body the proper function devoted to the interpolation which is `smooth.m`.

Methods

The principal goal in this section was to estimate angle excursion of hip (so the angle between the pelvis and the femur), knee (angle between femur and tibia) and ankle joints (angle between tibia and arbitrary line in the foot) starting from the laboratory stereophotogrammetry system. This is obtained by the application of three distinct methodologies:

- **Joint kinematics.** Considering G as the laboratory absolute reference system, each body segment's orientation can be described by a rotation matrix $\mathbf{R}_{S/G}$: this one contains as columns the versors of the solidal system associated with the segment. In biomechanics, it is usually customary to refer the orientation of a body segment with respect to the other, rather than expressing it in the laboratory reference. In particular, for multisegment parts of the body, like upper and lower limbs, it is customary to express the orientation of the distal segment with reference to the proximal one. Said $\mathbf{R}_{PS/G}$ and $\mathbf{R}_{DS/G}$ respectively the orientations of proximal and distal segments with respect to the absolute reference G, and said O_1 and O_2 respectively the origins of the solidal references, the position of a point P expressed in the solidal reference system of the proximal segment is given by:

  $$\vec{O_2P} = \mathbf{R}^T_{PS/G}\vec{O_1O_2} + \mathbf{R}^T_{PS/G}\mathbf{R}_{DS/G}\vec{O_1P}$$

  Usually, the matrix multiplying the second term on the right-hand side is noted as $\mathbf{R}_j = \mathbf{R}^T_{PS/G}\mathbf{R}_{DS/G}$ is said joint orientation matrix. This object describes the orientation of the distal segment with respect to the proximal one, and, given an angular convention and exploiting the orthogonality of $\mathbf{R}_j$, allows the retrieve the orientation description by three independent parameters.

- **Davis protocol.** The Davis protocol has become a standard in the evaluation of neuromuscular disorders and assessment of effects of post-operative orthopedic surgery [5]. Its value resides in systematic definitions to correctly execute gait tests with high precision and repeatably, pinpointing at each phase the correct procedures to collect data and process information. In our experience (points $1-2$ of Davis protocol [5]), it has produced the following datas for the subject:

  $$L = 0.920m \qquad X_{dis} = 0.110m \qquad D_{asis} = 0.210m$$

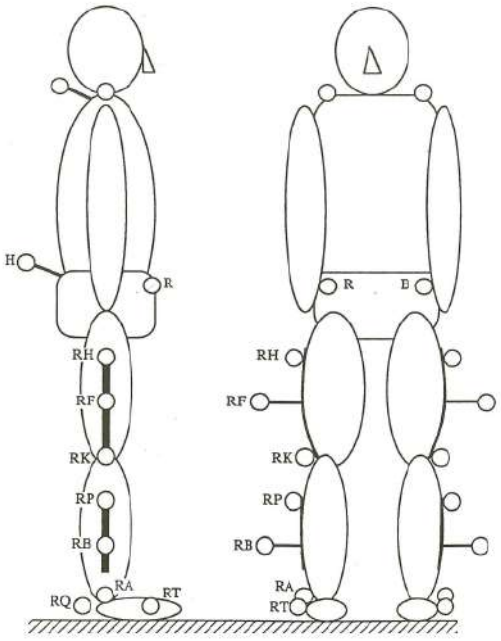

Figure 25: Marker positioning.

where L is the leg length of the subject, D_{asis} is ASIS-to-ASIS distance, and X_{dis} is the anterior/posterior component of the ASIS distance from the hip center.
Then the marker placement (3) was performed following 25 by the laboratory expert: 22 markers, among which 4 in wand, were located in precise anatomic landmarks. For each lower limb (except feet), three markers were placed allowing a univocal determination of an orientation tern, solidal with the segment. Then, the test was concluded with further two phases (points $4-5$), excluding the electromyography (6), which was collected from another test subject and discussed in the successive section. Both orientation matrices and origins of the terns shown in figure 25 have been calculated: in the first case, the general procedure used starting from three point P_1, P_2 and P_3 is:

$$\boldsymbol{\beta}_1 = \frac{1}{2}(P_1 + P_2) - P_3$$

$$\boldsymbol{\beta}_2 = P_2 - P_1 \quad \Longrightarrow \quad \mathbf{e}_{S,y} = \frac{\boldsymbol{\beta}_2}{\|\boldsymbol{\beta}_2\|}$$

$$\boldsymbol{\beta}_3 = \boldsymbol{\beta}_1 - (\boldsymbol{\beta}_1 \cdot \mathbf{e}_{S,y})\mathbf{e}_{S,y} \quad \Longrightarrow \quad \mathbf{e}_{S,x} = \frac{\boldsymbol{\beta}_3}{\|\boldsymbol{\beta}_3\|}$$

$$\mathbf{e}_{S,z} = \mathbf{e}_{S,x} \times \mathbf{e}_{S,y}$$

The tern $\{\mathbf{e}_{S,x}, \mathbf{e}_{S,y}, \mathbf{e}_{S,z}\}$ is orthonormal and attached to the segment and S, and in general this technique can be generalized for any body segment with three markers: hip, leg (left and right), and thigh (left and right). The rotation matrix expressed in the global system coordinates contains these versors as column, that is:

$$\mathbf{R} = [\mathbf{e}_{S,x}, \mathbf{e}_{S,y}, \mathbf{e}_{S,z}]$$

Nevertheless, in order to have the description of all these orientation terns, they must be considered together their origins, which are in turn expressed with respect to the global origin of the laboratory frame. The procedures proposed by [5] consider each segment separately:

- **Hip**. The so called "Hip centering algorithm" provides a center starting from the anatomical measures stuck in a set of regression equations which in turns provide:

$$\begin{cases} x_H = -0.95X_{dis} + 0.03L - 4 \\ y_H = s(-0.31X_{dis} - 0.096L + 13) \\ z_H = 0.05D_{asis} - 0.055L + 7 \end{cases}$$

  s is a parameter assuming -1 for the right side and 1 for the left. The hip center is expressed in the reference system solidal to the hip, hence the location expressed in the laboratory reference:

$$[\mathbf{x}_H]_G = \mathbf{R}_{hip}\,[\mathbf{x}_H]_L + \left[\frac{1}{2}(\vec{OP}_1 + \vec{OP}_2)\right]_G$$

  where P_1 and P_2 indicates the global expression of the left and right ASIS.

- **Knee**. For the knee:

$$\begin{cases} x_K = 0 \\ y_K = s(r_{marker} + w_{knee}) \\ z_K = 0 \end{cases}$$

  where s indicates the sign related to the side of the leg considered, r_{marker} (which is zero in this case) is the marker radius (in meters) and $w_{knee} = 0.105m$ is the knee width measurement (in meters). As in the previous point:

$$[\mathbf{x}_T]_G = \mathbf{R}_{knee}\,[\mathbf{x}_T]_L + \left[\vec{OP}_1\right]_G$$

  where $P1$ is the knee marker position in the laboratory reference.

– **Ankle**. For the ankle:

$$\begin{cases} x_A = 0 \\ y_A = s(r_{marker} + w_{ankle}) \\ z_A = 0 \end{cases}$$

where s has the usual role as in the previous ones, $w_{knee} = 0.105m$ and $r_{marker} = 0$. Then:

$$[\mathbf{x}_A]_G = \mathbf{R}_{ankle} [\mathbf{x}_A]_L + \left[\vec{OP_1}\right]_G$$

where $P1$ is the malleolus marker on the ankle with respect to the global reference.

At the end of this phase, we have expressed all the orientations terns and related center movement in the laboratory system for each sample acquired by the TVC system. Therefore, the knowledge of every rotation matrix $\mathbf{R}(t)$ allows the computation of every joint rotation matrix, hence the calculation of joint angles.

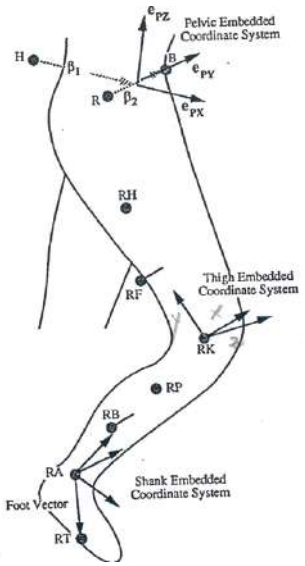

Figure 26: Embedded coordinate systems to each segment.

- **Grood and Suntay convention**. An angular convention is the choice of at least three parameters describing the orientation of a rigid body with respect to a global reference (laboratory). In Biomechanics, the convention chosen is a Cardanic terns of angles, that is to say, the orientation is determined as elementary rotations with respect to the principal axes of the proximal segment. According to [6], the convention states:
  - First rotation β about the flexion-extension axis.
  - Second rotation α about the abduction-adduction axis.
  - Third rotation γ about the longitudinal axis of the distal segment.

Since the elementary rotations are made by fixed axes, the final orientation matrix of a distal segment with respect to the proximal one is given by:

$$\mathbf{R}_j = \mathbf{R}_{Y,\beta}\mathbf{R}_{X,\alpha}\mathbf{R}_{Z,\gamma} = \begin{bmatrix} R_{11} & R_{12} & R_{13} \\ \cdot & R_{22} & R_{23} \\ \cdot & \cdot & R_{33} \end{bmatrix}$$

This matrix belongs to the $SO(3)$ rotation group, then it is possible to retrieve the tern identifying $\mathbf{R}_j$. Then the Cardanic angles coincides with those of physiological interest in gait analysis. The angles of ab-adduction, flexion-extension, and internal-external rotation at each joint are given by:

$$\alpha = -\sin^{-1}(R_{23}) \tag{28}$$

$$\beta = \sin^{-1}\left(\frac{R_{13}}{\cos\alpha}\right) \tag{29}$$

$$\gamma = \sin^{-1}\left(\frac{R_{21}}{\cos\alpha}\right) \tag{30}$$

These three methods are implemented in MATLAB following the flowchart in 27:

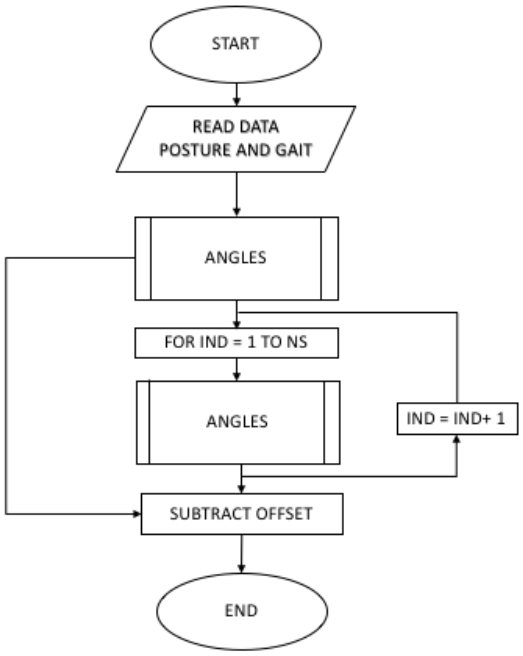

Figure 27: Flow diagram of `calculatedavis.m`

The block *ANGLES* is the cascade of the aforedescribed methods, and the whole algorithm described in figure is englobed in the main program `calculatedavis.m`. First of all, off-set

angles are required: they indicate the own postural configuration of the subject, to which are referred each excursions of segments; hence they are gained by data acquired when the subject is in quiet stance. As it can be seen in 27, the same subroutine to calculate α, β and γ is used for these off-set angles, but out of the cycle in order to be computed just once. The core of *ANGLES* is made by the three functions `landmarks.m`, `define_ECS.m` and `groodsuntay.m`, which sequentially. In particular, the first one select correctly from camera files and retrieves the position of each markers correspondent to the related segment. Then, these position are processed by `define_ECS.m`, which computes all the rotation matrices associated with every segment, along with their centers. Finally, `groodsuntay.m` calculates the joint matrix from the outputs of the previous function; in particular, it retrieves the orientation matrices of the proximal and distal segment at the joint considered, calculating the joint matrix, hence the angles according to [6], using the formulas (28),(29) and (30). To be noted, the foot segment is provided only by a vector called foot line, therefore it is impossible to define a joint matrix. The solution has been found by projecting the foot line vector in the xz plane defined by the shank embedded system. The plantar flexion and dorsiflexion angle (the only needed in this analysis) is then found as the angle between $\mathbf{e}_{3,A}$ and the projected vector. The following equation describes the projection of the foot line $\mathbf{v}$ as:

$$\mathbf{v}_p = \mathbf{P}\mathbf{v}$$

where $\mathbf{v}_p$ is the projected vector and $\mathbf{P} = \mathbf{I} - (\mathbf{e}_{2,A} \otimes \mathbf{e}_{2,A})$ is called the orthogonal projector. Then, after normalization of $\mathbf{v}_p$, the ankle angle is given by:

$$\beta_A = \cos^{-1}(\mathbf{v}_p \cdot \mathbf{e}_{3,A})$$

These operations are applied iteratively for every instant of time where the acquisition is available (indicated as *IND* in 27). Then, the final outcome is a time-series of angular displacements at each joint, accounted for the three rotation axis defined by the Cardanic convention.

Discussion and conclusions

Besides the algorithms for gait angles computation, the whole graphics part is controlled by `gaitui.m`, which contains the GUI part related to gait analysis. Clicking on *GAIT* button in the start window, a dialog box opens letting the user two possible options:

Figure 28: Gait analysis options

Choosing the first option, the flexion-extension angles found are in the following picture:

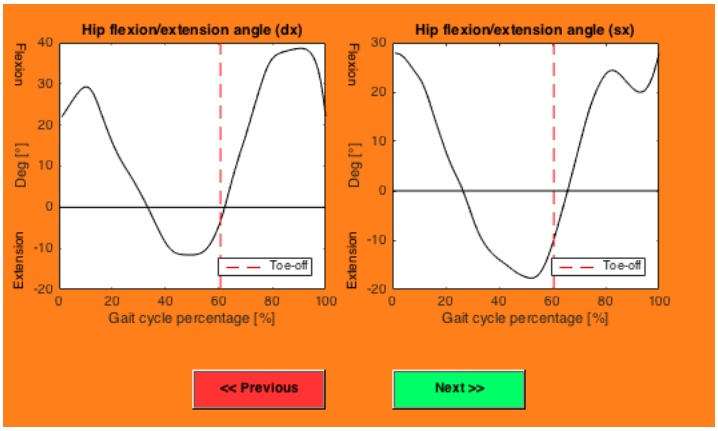

Figure 29: Hip flexion/extension

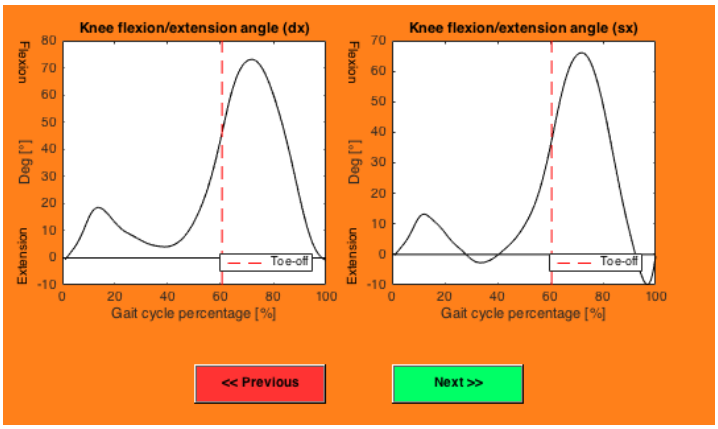

Figure 30: Knee flexion/extension

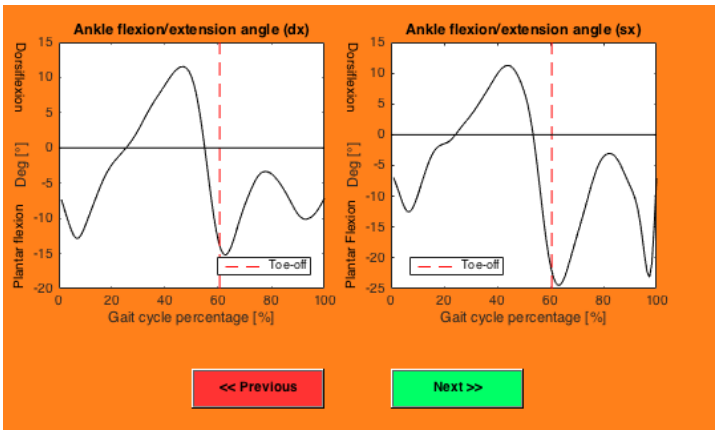

Figure 31: Ankle plantar flexion/dorsiflexion

The trends of joint angles obtained in figures 29,30 and 31 are much close to reference ones taken from [4]:

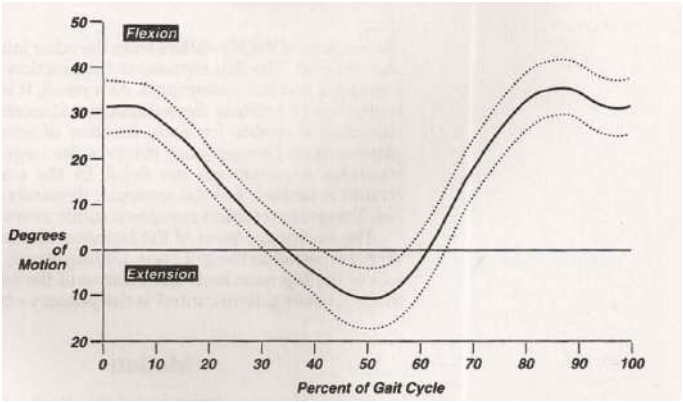

Figure 32: Hip joint

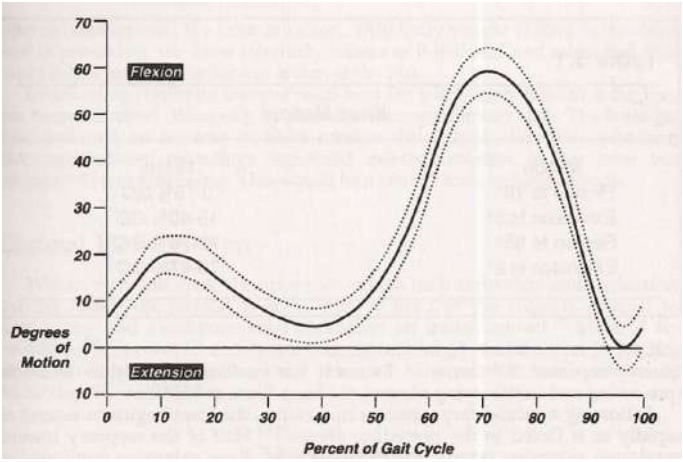

Figure 33: Knee joint

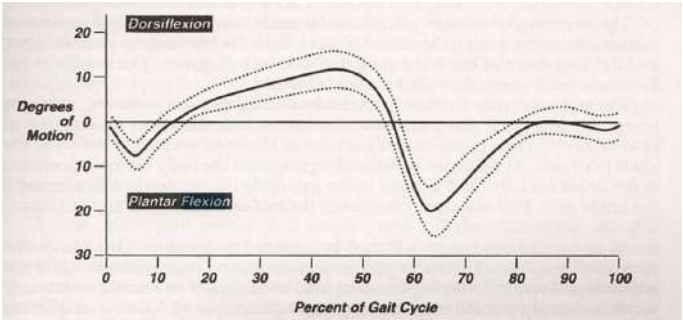

Figure 34: Ankle joint

The toe-off phase, indicated in the previous picture by the red line, has been taken from extra platform acquisitions, which stop acquiring as the foot begins the swing phase. These samples were also used in the second option, to obtain Butterfly diagrams of the gait cycle:

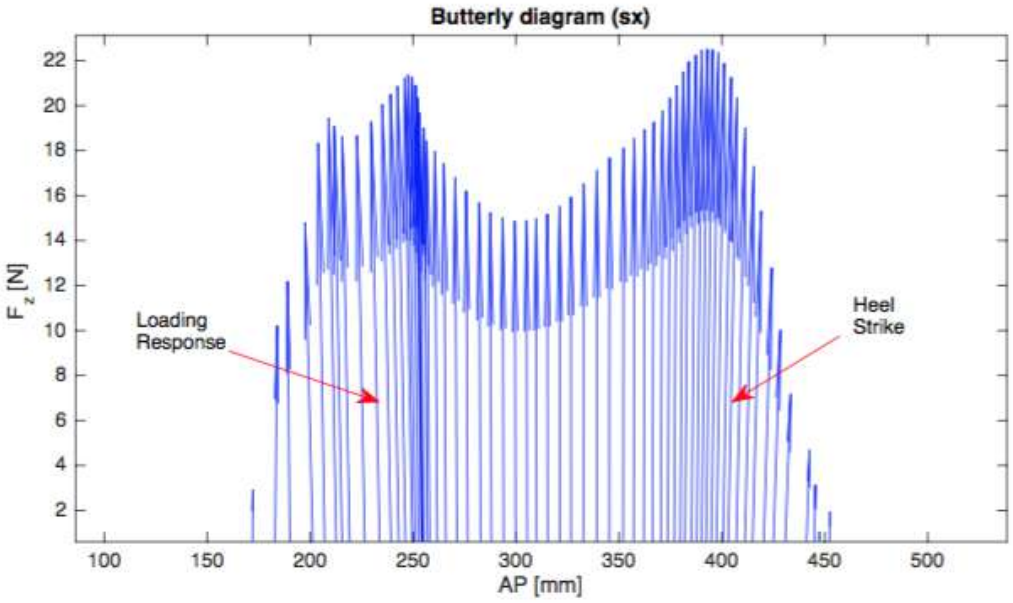

Figure 35: Butterfly diagram of the left foot from the same trial of 29,30, 31.

In figure 35, it can be appreciated the characteristic shape, showing a ground reaction force increasing during loading response, decreasing then for the toe-off by controlateral side foot, and then again increasing in the heel strike to rapidly vanish in the pre-swing phase.

EMG

Electromyography (EMG) is a diagnostic tool to assess the health of muscles and nerve cells controlling them (motor neurons). Motor neurons transmit electrical signals that cause muscles to contract: an EMG test translates these physiological activations into numeric signals, which in turn are rendered with charts, screen monitors, or sound devices to clinician and specialists for interpretation and possible anamnesis/diagnosis. Muscles are directly controlled by motor neurons endings starting directly from the cerebral cortex and descending through spinal cord pathways. A motor unit (MU) is made up of a motor neuron and a bundle of skeletal muscles. Groups of motor units often work together to coordinate the contraction of a single muscle:

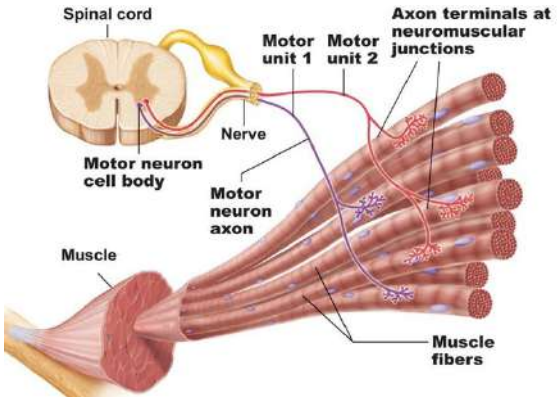

Figure 36: Motor unit.

The force output of the muscle is modulated by the recruitment of motor units and the regulation of their firing rates. As the excitation increases, motor units are progressively recruited, and all the active motor units simultaneously increase their motor unit action potential (MUAP) firing rates. In this fashion, earlier recruited motor units have greater firing rates than later ones; in addition, every MUAP has a triphasic pattern with shape and size depending on the relative orientation of fiber-electrode, strength and type of the MU [8]. All these factors summed together contribute to the final EMG morphology. The transducers for EMG are tiny devices called electrodes which transmit or detect electrical signals. There are two techniques to record the signal: the first one is an invasive technique and is performed using needles electrodes under live

skin. The second one is a non-invasive and is done with superficial electrodes (sEMG), which have their real value on cheapness and ease to use versus a poor localization of the electrical activity causing muscle contraction. EMG results can reveal nerve dysfunction, muscle dysfunction or problems with nerve-to-muscle signal transmission. It is possible, also, to perform it during other activities, for example during gait analysis, to determine muscle activation during gait phases as in our laboratory experience.

Materials

The experiment was conducted in the laboratory of movement analysis of UNIVPM (faculty of engineering). The study was carried out on a 24-year-old male subject in healthy condition. Three different kind of signals was recorded using three different sensors:

- Electrogoniometric sensor (figure 37), placed on the knee joint to evaluate the angular variation associate to a specific gait phase.
- Basographic sensor (figure 38), which consists three sensors placed under the foot, more precisely on the heel, on the first and five metatarsal head and they are used to underline the foot-ground contact. Signal output is composed by four level (foot-flat FF, push-off PO, swing SW, brake BR) that represent the different phase of the gait.
- EMG electrodes, applied on a specific location according to the European project SENIAM (Surface EMG for Non-Invasive Assessment of Muscles).

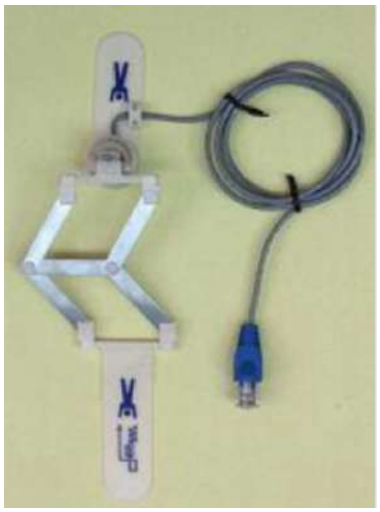

Figure 37: Goniometric sensor.

Figure 38: Basographic sensors.

A total of five muscles were recorded: Tibialis Anterior, Gastrocnemius Lateralis, Rectus Femoris, Hamstrings, Vastus Lateralis:

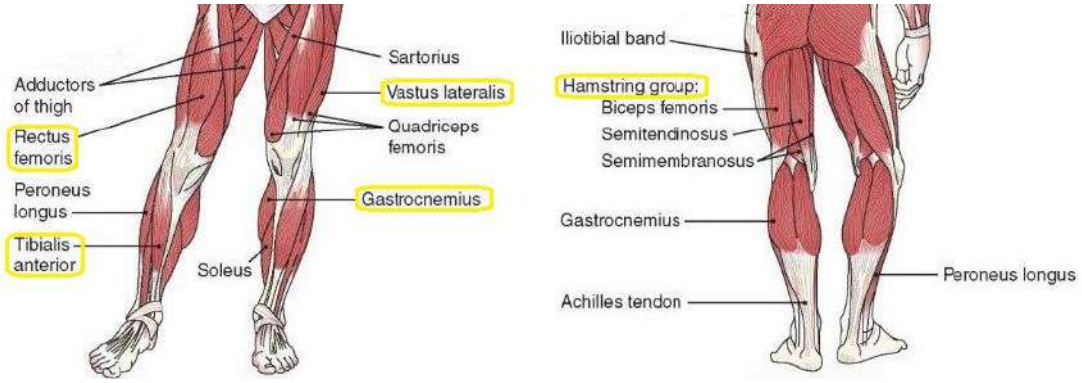

Figure 39: Leg muscles.

The 16 signals were recorded by a device (patient unit) and then processed with a software interface called STEP 32, that allows a simultaneous processing of at most 32 channels.

Methods

The aim of this section is to estimate the on-off timing of human skeletal muscles during walk. The main tools used can be subdivided in these three successive signal processing steps:

- **Finite-state machine.** A finite-state machine (FSM), or simply state machine, is a mathematical model of computation. It is an abstract machine that can be in exactly one of a finite number of states at any given time. The FSM can change from one state to another in response to some external inputs. The change from one state to another one is called transition. An FSM is defined by a list of its states, its initial state, and the conditions for each transition. In this case, we have used the FSM to determine the step by employing the raw basographic signal.
  The basographic signal represent four phases of the gait cycle: it starts with the Heel Contact (0-5 %), then there is the Flat-Foot contact (6-47 %), the Push-Off (48-63 %) and the last phase: the Swing (64-100 %)41.
  These four level is obtained by the on-off combination of three electrode (more precisely switch buttons) under the feet, located on the heel, first and fifth metatarsal head 40 (off: electrode pushed; on: electrode unpressed).

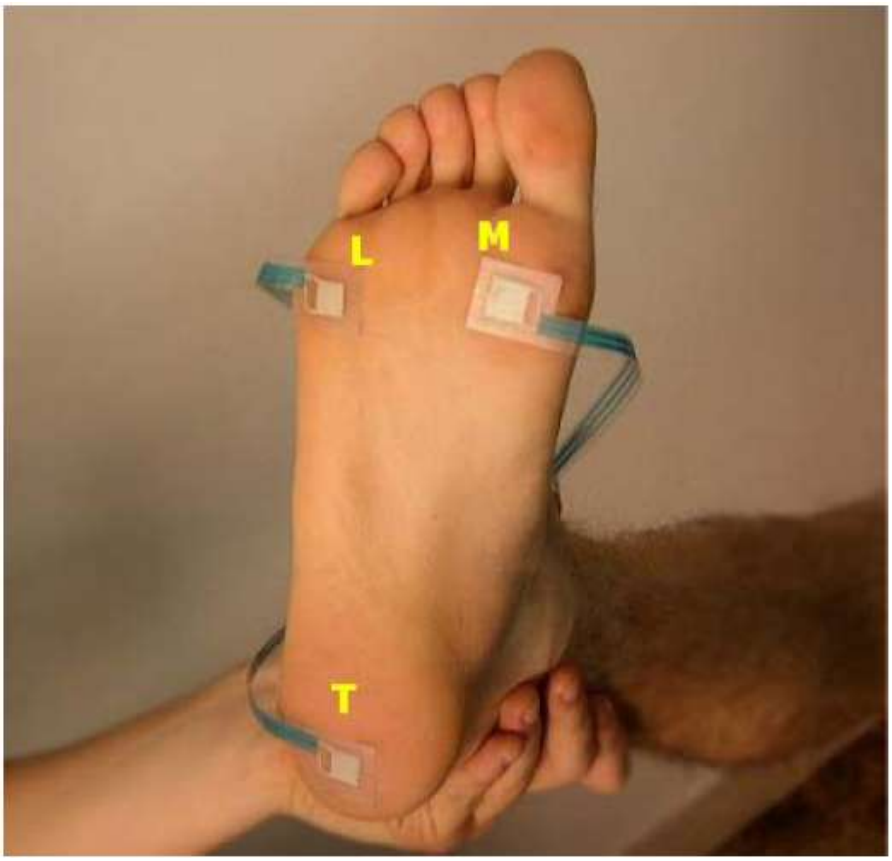

Figure 40: switch buttons location under the foot

As we can see in the picture above 40 the electrodes are T,L,M and the level are given as follow:

- H, T pushed;
- F, all pushed;
- P, L and M pushed;
- S none pushed.

These four level of the basographic signal were set as state of the machine and the value corresponding to the heel contact (the first phase of gait) as initial value. An additional feature related to this state machine approach is the retrieval and counting of steps.

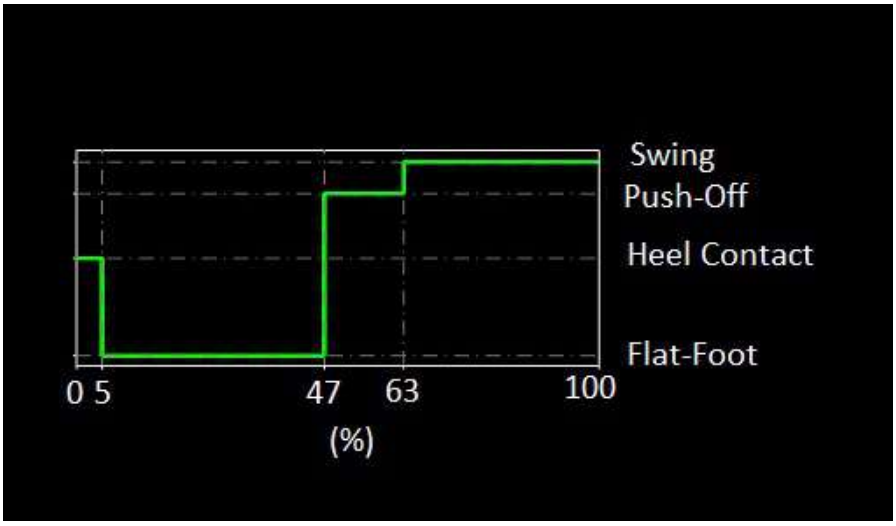

Figure 41: basographic signal with gait phases

- **Wavelet analysis.** Muscle activity is recognized on the basis of the presence of MUAPs in the sEMG signal. On the whole, surface EMG signal can be described as a summation of MUAP trains (MUAPT) and a share related to noise:

$$\text{MUAP}_j(t) = \sum_i k_j f\left(\frac{t-\theta_{ij}}{\alpha_j}\right) + n(t)$$

where $f(t)$ is the function describing the j-th MUAP, k_j is an amplification factor, θ_{ij} is the relative time localization in the train of pulses and α is a scaling factor [9]. The noise share $n(t)$ is usually modeled as a stochastic process describing the several sources of noise affecting the signals of muscular activation, which is usually confusing with the desired signal due to their similar morphology. In addition to this, the non-stationarity of the signal at issue has led to novel approaches to extract the useful component of the sEMG signal. Wavelet transform, which is part of the time-frequency DSP techniques, has been successfully applied [9], allowing a "scattered" representation of the signal, that is, a multilevel representation showing signal components occurred only at particular frequencies and when matching a particular shape. The continuous wavelet transform is defined as:

$$\mathbf{CTW}_x^{\psi}(s,\tau) = \frac{1}{\sqrt{s}} \int_{-\infty}^{+\infty} x(t)\psi^*\left(\frac{t-\tau}{s}\right) dt$$

where $\psi(t)$ is said mother wavelet and the parameter $(a,b) \in (0,+\infty) \times (-\infty,+\infty)$ are respectively the scale and localization parameters of the wavelet ψ. Any function derived

by ψ and the couple (a, b) is said daughter wavelet, and it reads:

$$\psi_{a,b} = \frac{1}{\sqrt{a}}\psi\left(\frac{t-b}{a}\right)$$

This particular transform gives a representation of the signal at any frequency s, to which is associated all the signal components with similar features to the daughter wavelet at the current frequency. Indeed from the definition, it is possible to appreciate that, given a mother wavelet, the wavelet transform applies a filter with a cut-off frequency varying with a and a impulsive response of the filter depending on ψ. The CTW has its strength in the capability of highlighting in the time-frequency plane (scalogram) zones containing signal portions with desired trends from noises. Nevertheless this representation is continuous and redundant, and it heavily depends on the choice of the mother wavelet. These problems were successfully solved by the multiresolution analysis [7], which allows an easy and recursive implementation of wavelet transform (DWT) as bank of filters. The fundamental result is known as the wavelet series, which reads:

$$x(t) = \sum_{k\in\mathbb{Z}} S_{i_0,k}\varphi_{i_0,k}(t) + \sum_{i=i_0}^{+\infty}\sum_{k\in\mathbb{Z}} W_{i,k}\psi_{i,k}(t) = x_{i_0}(t) + \sum_{i=i_0}^{+\infty} d_i(t)$$

where $x_{i_0}(t)$ is said approximation of the signal at frequency i_0, while $d_i(t)$ is said detail of the signal at scale i_0. This decomposition is univocal, as the functions $\varphi_{i,k}$ (scaling function or father wavelet) and $\psi_{i,k}$ (mother wavelet) can be used to constitute separate basis of two orthogonal spaces. Said this, the coefficients $\mathbf{c}_{i_0} = [S_{i_0,1}, \ldots, S_{i_0,k}]$ and $\mathbf{d}_i = [W_{i,1}, \ldots, W_{i,k}]$ can be easily found using the following scheme: In this view, in order to

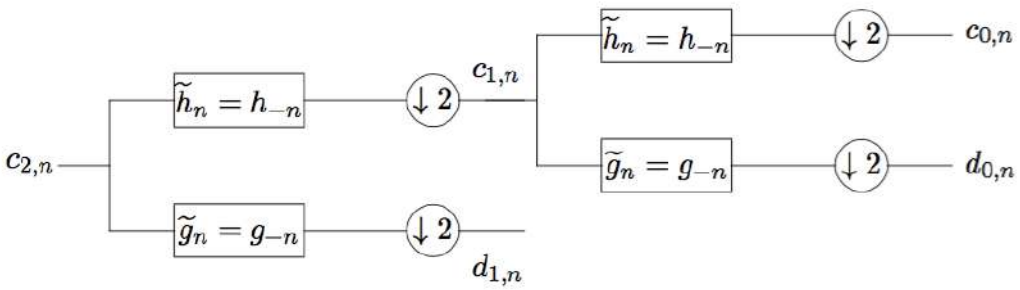

Figure 42: Analysis bank filter.

completely define the wavelet series, all the coefficients are retrieved by applying recursively to them a couple of (possibly FIR) high-pass and low-pass filters, g_n and h_n, known as

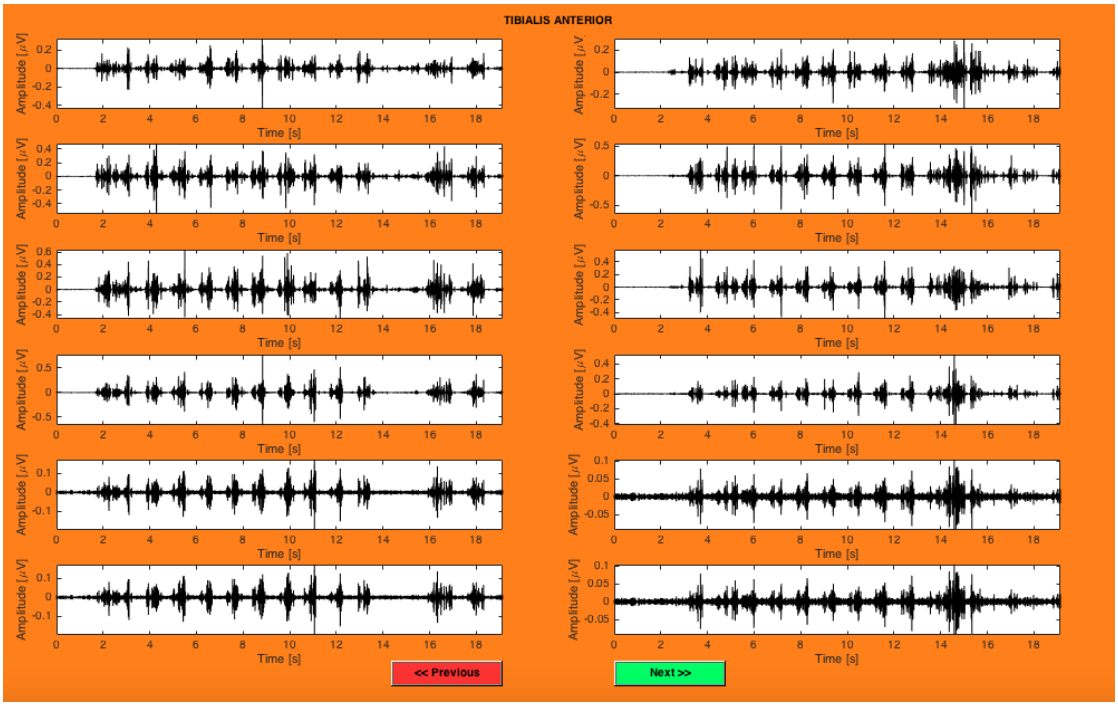

Figure 43: EMG details

wavelet filters, at each level (analysis bank):

$$S_{i-1,n} = \sum_{k\in\mathbb{Z}} S_{i,k}\tilde{h}_{2n-k} \tag{31}$$

$$W_{i-1,n} = \sum_{k\in\mathbb{Z}} S_{i,k}\tilde{g}_{2n-k} \tag{32}$$

From this scheme, all approximations and details until scale i are known, and they can be used to analyze the signal in its scattered representation: usually the approximations take in account of the low cycle trends inside the signal, while the details are used to classify high-frequency contents within the signal. Furthermore, it is possible also to reconstruct entirely the signal (synthesis bank) using the same wavelet filters. The algorithm, proposed by Mallat et al. [7], usually formulates as follow. Given a signal $x[n]$:

1. Initialize $\mathbf{S}_{i_0}$ with $x[n]$, with $i_0 = \log_2 L$ (L number of samples of $x[n]$).
2. Use (28) and (29) to obtain $\mathbf{S}_{i_0-1}$ and $\mathbf{W}_{i_0-1}$.
3. Iterate from step 2.

In our study, six level of details were used (neglecting the approximation), producing the outcomes in figure 43 from the EMG data set provided by the experiment.
The chosen wavelet mother is the *'dB4'* (Daubachies family), which has the following

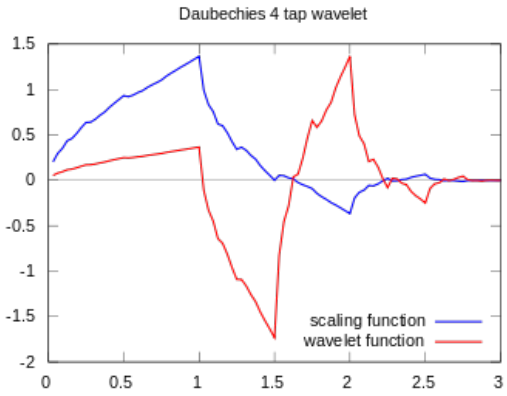

Figure 44: Daubachies 4

characteristic waveform in figure 44.

- **Threshold algorithm.** Once the signal is split in its multiple details, it is possible to define a procedure to define from these a binary signal, known as activation, which is set high (level 1) in correspondence of the beginning of the contraction of the muscle (or muscular group) related to the respective surface electrode, and is set low (level 0) when the contraction ceases. Following the work of Merlo et al. [9], the amplitude threshold is defined starting from the following function:

$$\eta(t) = \max_{s}\{\mathbf{DWT}(s,t)\}$$

Basically, this function acquires the maximum value of the correspondent sample at time k among all the details considered. Then, the threshold is defined as:

$$M = \max\{\eta(t)\} \qquad 0 < t < T_n \tag{33}$$

$$\text{TH} = \gamma \cdot M \tag{34}$$

where $\gamma > 1$ is a characteristic parameter of the considered muscle. As shown above, the amplitude threshold is defined on the initial noisy segment of the signal where EMG activity is absent, which goes from $0 < t < T_n$, with T_n declaring the end of this segment. After the computation of the threshold, the revealed activation is set high for the time periods during which exceeds the threshold TH and zero otherwise. If the SNR is high, the choice of $\gamma > 1$ is not critical, due to the great amplitude difference between EMG signal and noise. If the SNR is low, a low value $\gamma > 1$ of becomes a conservative choice.

Discussions and Conclusions

In this section, the GUI was organized with two possible options: the first one, to explore all the six details for each muscle (see figure 41), in both left and right leg, and the second one to study all EMG signals in correspondence of the Basographic and with their related activation:

Figure 45: EMG options.

For what concerns the second option, at first glance the GUI window presents as shown in figure 43: the first two are the basograph for both left and right feet, with context menus to select the first step and the number of following steps to be shown in the basograph. This choice also modify the appearance of the other two charts below, which indicates sEMG for one muscle at time (a couple of back-forward buttons are provided to scroll among the five muscles considered in this study). Furthermore, there is a radio button per basograph, showing the unprocessed basographic signal prior the state-machine routine. As said before, the second pair of graphs indicate the sEMG recordings for both left and right leg. The "ACT" button allows the superimposition of the activation for that muscle.

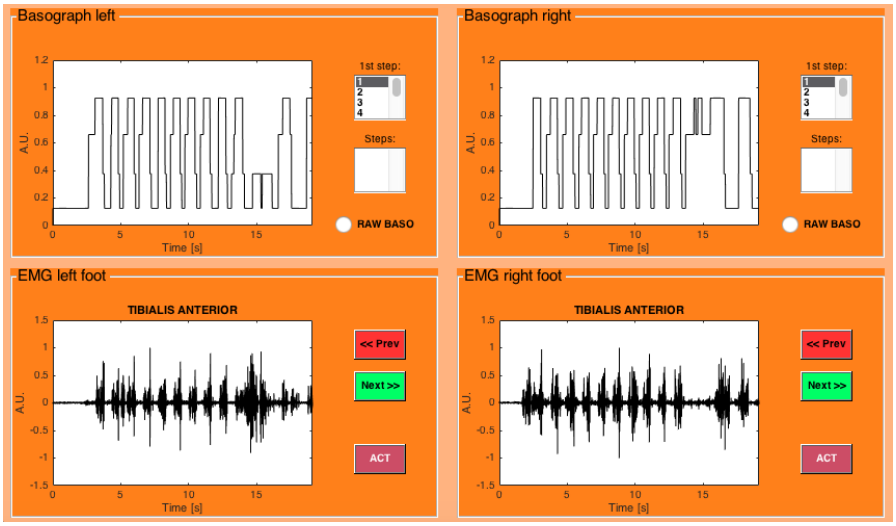

Figure 46: Opening screen for option "Activations".

The implementation of the algorithms follows the methods outlined in the previous section. In particular, the post-processing of the activation signal was done merging all the square waves far one each with the other less than 200 ms, and disregarding the isolated events with a shorter duration than 130 ms. Indeed, the activation obtained are following indeed the EMG signal, as

shown in the following set of figure for every muscle (the first five ones for left leg, the remaining ones for right leg):

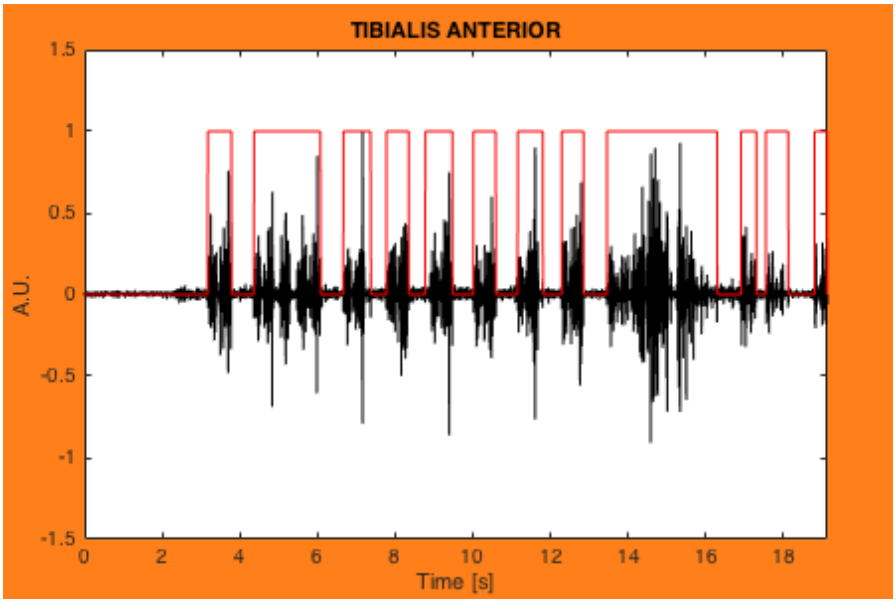

Figure 47: figure
Left tibialis anterior.

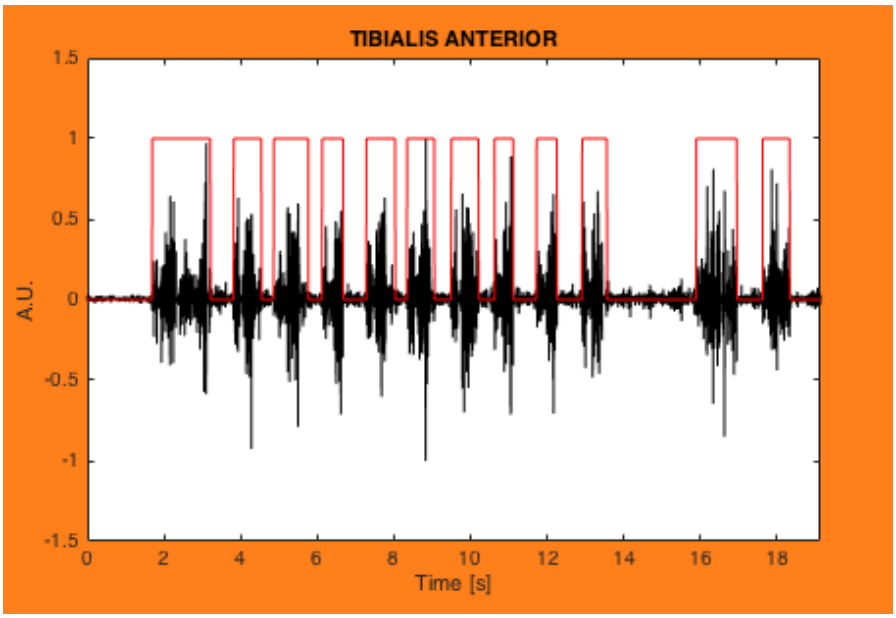

Figure 48: figure
Right tibialis anterior.

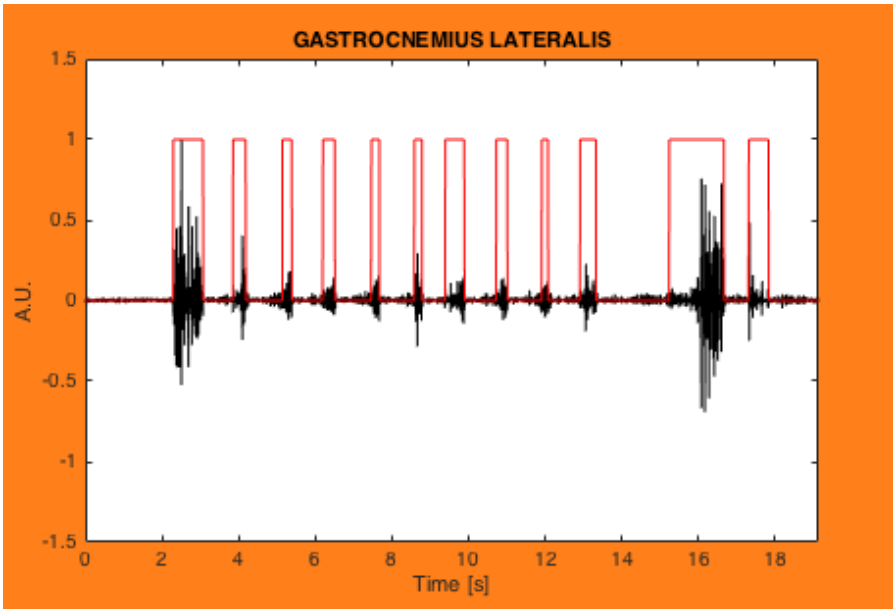

Figure 49: figure
Left Gastrocnemius.

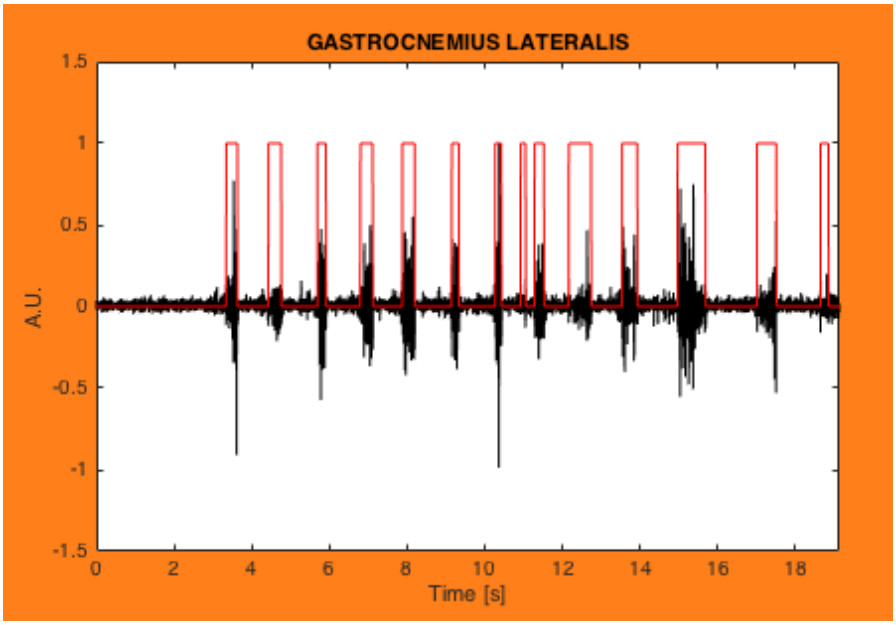

Figure 50: figure
Right Gastrocnemius.

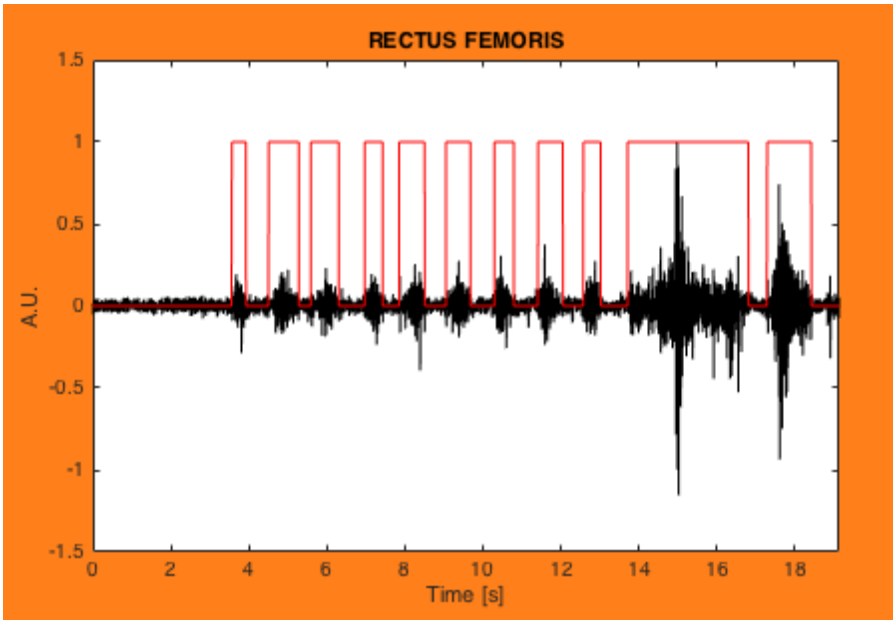

Figure 51: figure
Left rectus femoris.

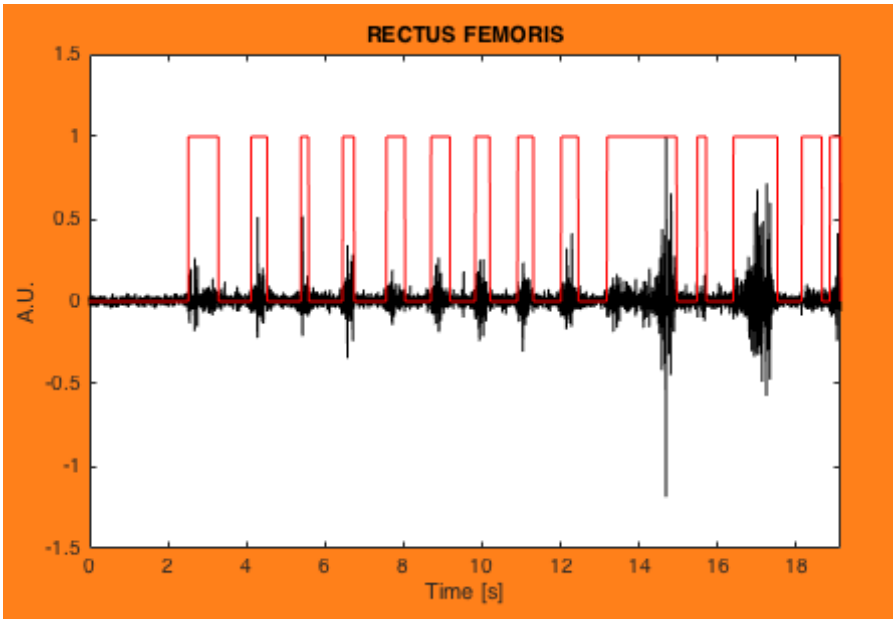

Figure 52: figure
Right rectus femoris.

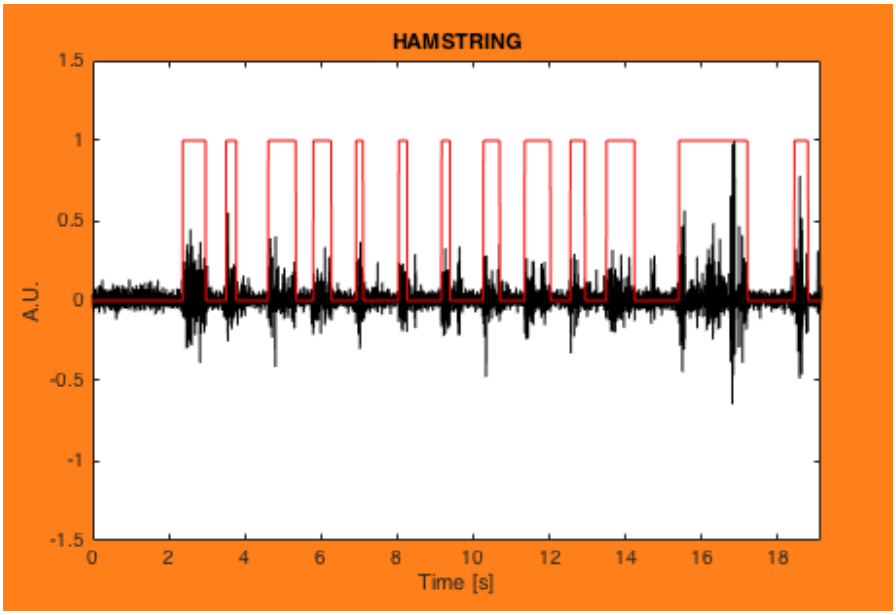

Figure 53: figure
Left hamstring.

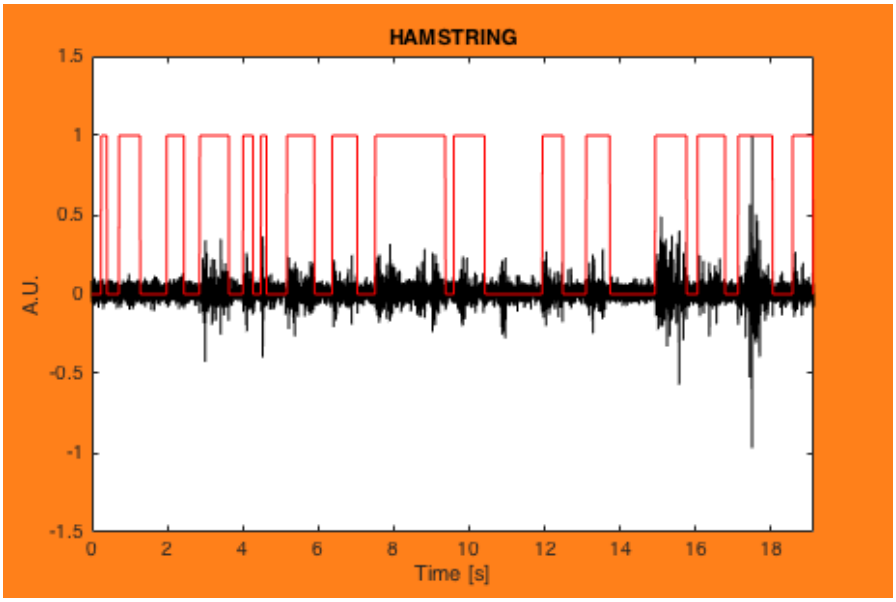

Figure 54: figure
Right hamstring.

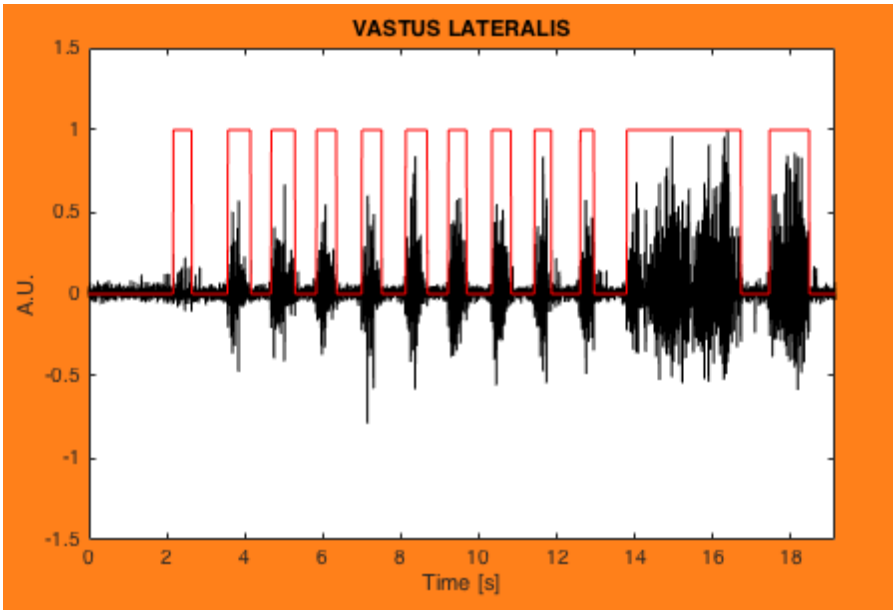

Figure 55: figure
Left Vastus Lateralis.

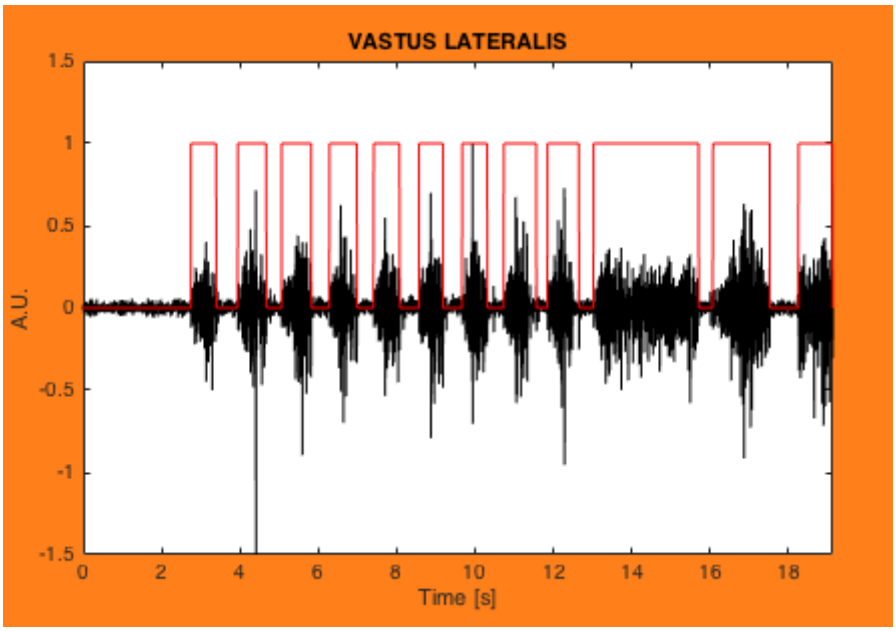

Figure 56: figure
Right Vastus Lateralis.

The main limit of this implementation are the threshold algorithm parameters: T_m (time period under which nearby activation are merged), T_d (minimum time period of isolated events) are in contrast to the post processing proposed by [9], which suggests $T_m = 125$ ms and $T_d = 5$ ms. In addition, it is difficult to implement automatic processing to obtain T_n, which in our study was determined by a graphical inspection of the EMGs recordings, which have a common noise segment of $T_n = 1500$ ms. In a similar way, the γ parameter was determined singularly for every muscle, in both left (L) and right (R) legs, by repeated attempts:

$$\boldsymbol{\gamma}_L = \begin{bmatrix} 4 \\ 2.6 \\ 1.8 \\ 0.8 \\ 2.4 \end{bmatrix} \qquad \boldsymbol{\gamma}_R = \begin{bmatrix} 3 \\ 3 \\ 1.5 \\ 0.8 \\ 2 \end{bmatrix}$$

As reported in [9], in conditions of high SNR the choice of $\gamma > 1$ is not affecting the revelation of the muscular activation. Thus, the major drawback of this approach is the parameter adjustment by graphical inspection of the activation overlapped on the EMG trends, which should be replaced by automatic preceding based on signal indexes and morphology, rather than on user-dependent adjustments which undermine the robustness of the algorithm, making it poorly repeatable and trial-sensitive. Despite the absence of an analytic parameter determination, the muscular activation in our study are acceptable accordingly with the occurring of MUAPs and the gait phases, showing a partial loss of accuracy for both hamstrings muscles, which are well-known poor SNR signals. In force of our findings, we can confront EMG activations with the kinesiology of leg muscles. Referring to the pictures 57, 58 from [4], we see that the Tibialis Anterior contraction occurs in the heel contact and push-off/ swing so in the initial phase and the last phase while the Gastrocnemius (its antagonist muscle) fires in the flat-foot contact.

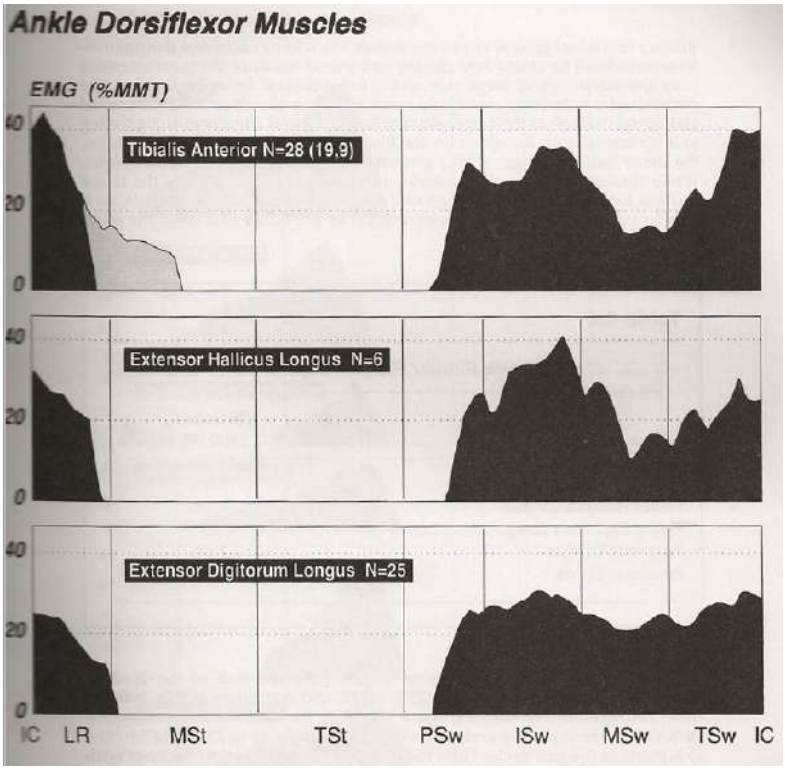

Figure 57: Ankle dorsiflection muscles, normal mean intensity and timing during free walking

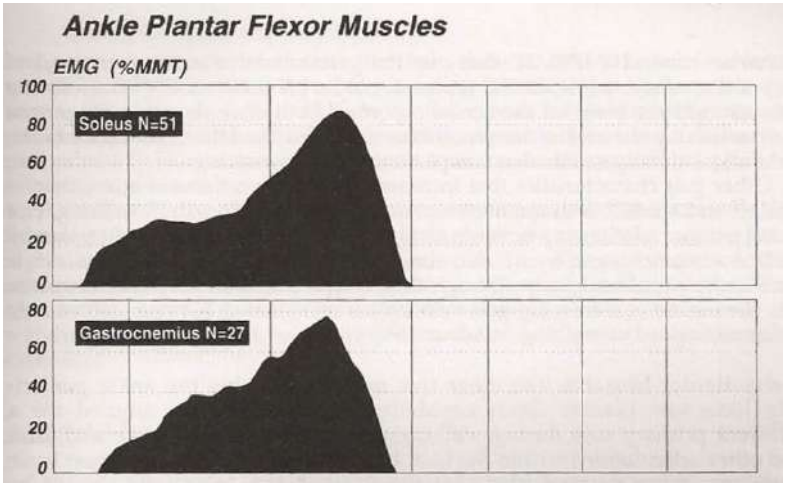

Figure 58: Ankle plantarflection muscles, normal mean intensity and timing during walking

The activations found for those two muscle occur correctly in their related phases of the gait cycle, as it is possible to see in the pictures 59 60.

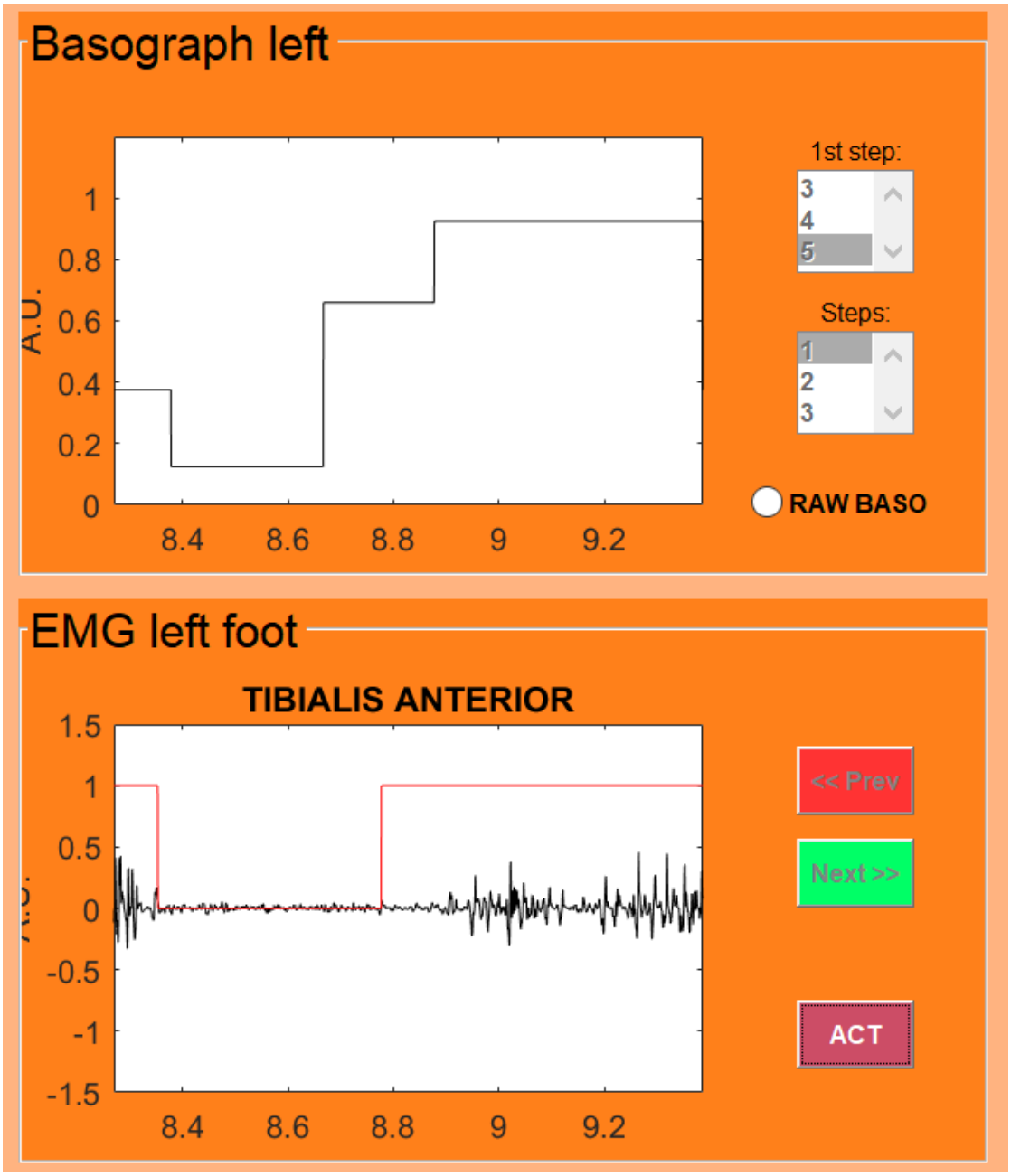

Figure 59: Tibialis Anterior activation

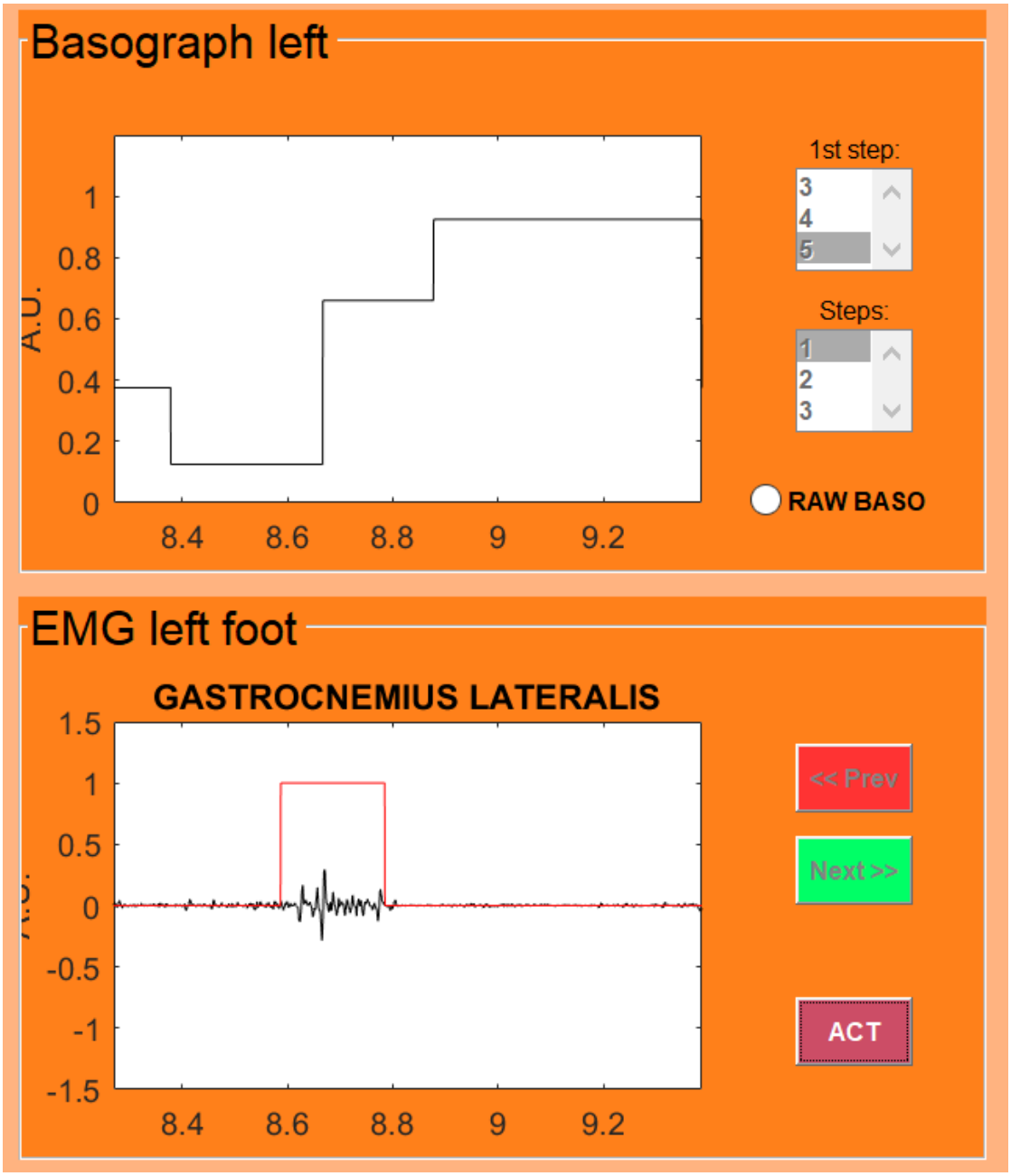

Figure 60: Gastrocnemius activation

The activation patterns measured of the muscles of quadriceps femoris group, such as Vastus Medialis (VM), Vastus Lateralis (VL), and Rectus Femoris (RF) are slightly in contrast with what reported in [4]. The activations are the following: the Vastus turns on similar to the Tibialis Anterior: from heel strike to mid-stance and from terminal swing to the following initial contact.

These two activation modalities found for the Vasti is expected in [4], and is required to generate tension in terminal swing in preparation for weight bearing at initial contact and to control knee flexion during weight acceptance 61. The Rectus Femoris turns on three times, at the beginning of gait cycle, around stance-to-swing transition and in the terminal swing 62. In a further percentage of strides, the pattern is similar, except for the activation around stance-to-swing transition that splits into two (or three) small activations, between heel-off and foot-off.

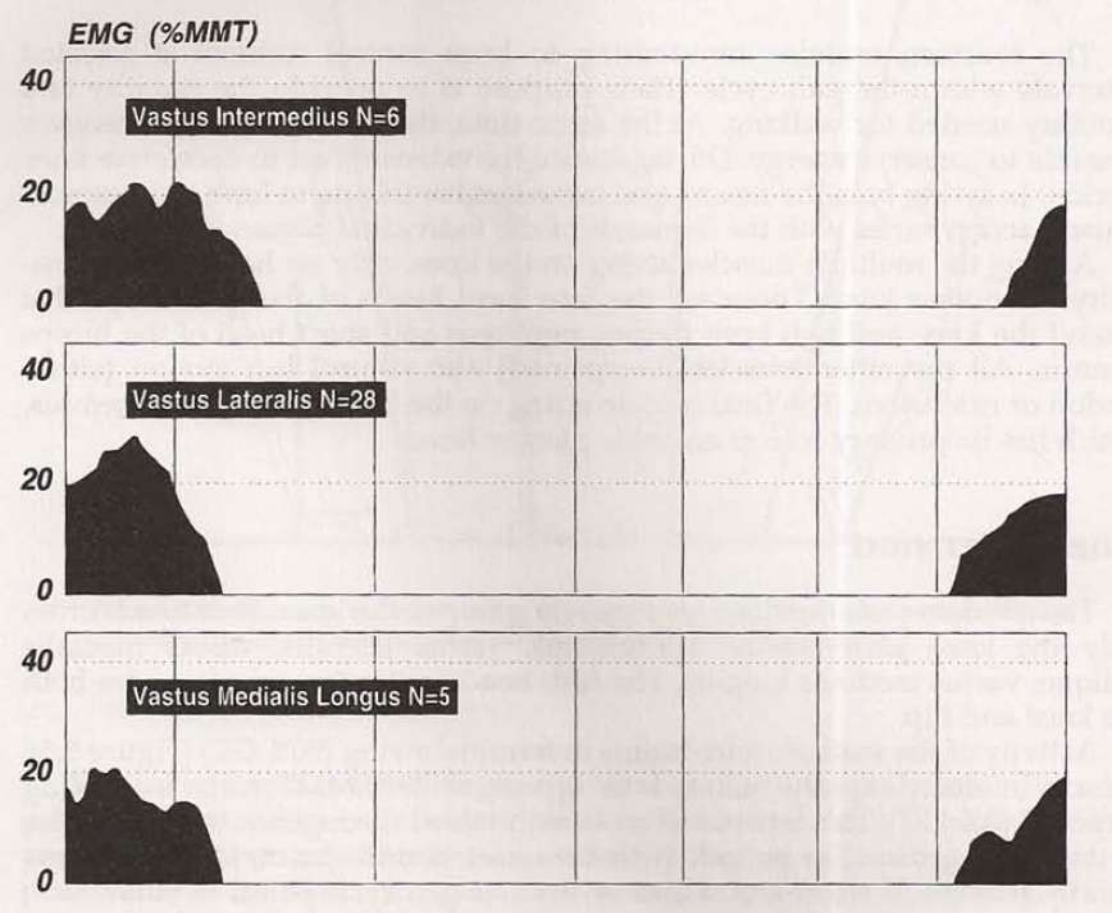

Figure 61: Knee extensor muscles, normal mean intensity and timing during free walking (Vasti)

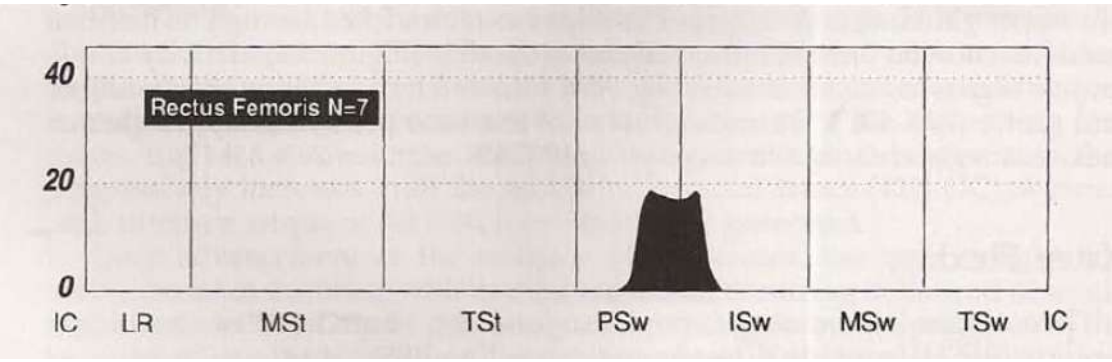

Figure 62: Knee extensor muscles, normal mean intensity and timing during free walking (Rectus Femoris)

In our case the Vastus Lateralis work correctly 63; instead, the Rectus Femoris does not active in the stance to swing transaction but only in the heel contact and end-swing 64. This absence of signal has been reported also by more recent fine-wire studies [11]. An explanation to this disagreement has been suggested by the observation that the apparent RF activity commonly recorded during loading response using sEMG is actually the result of cross-talk from the surrounding Vastii [12][13].

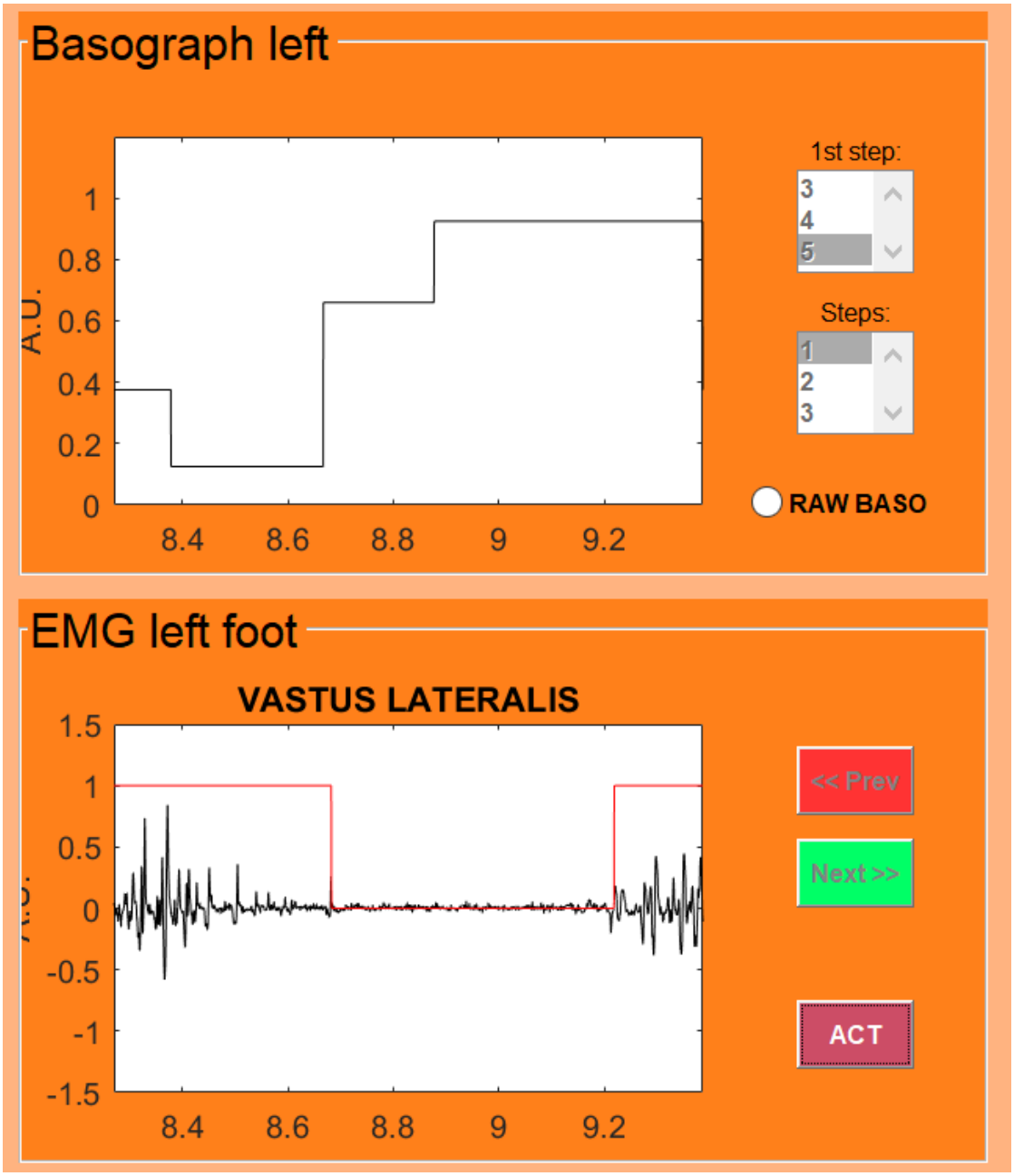

Figure 63: Vastus Lateralis

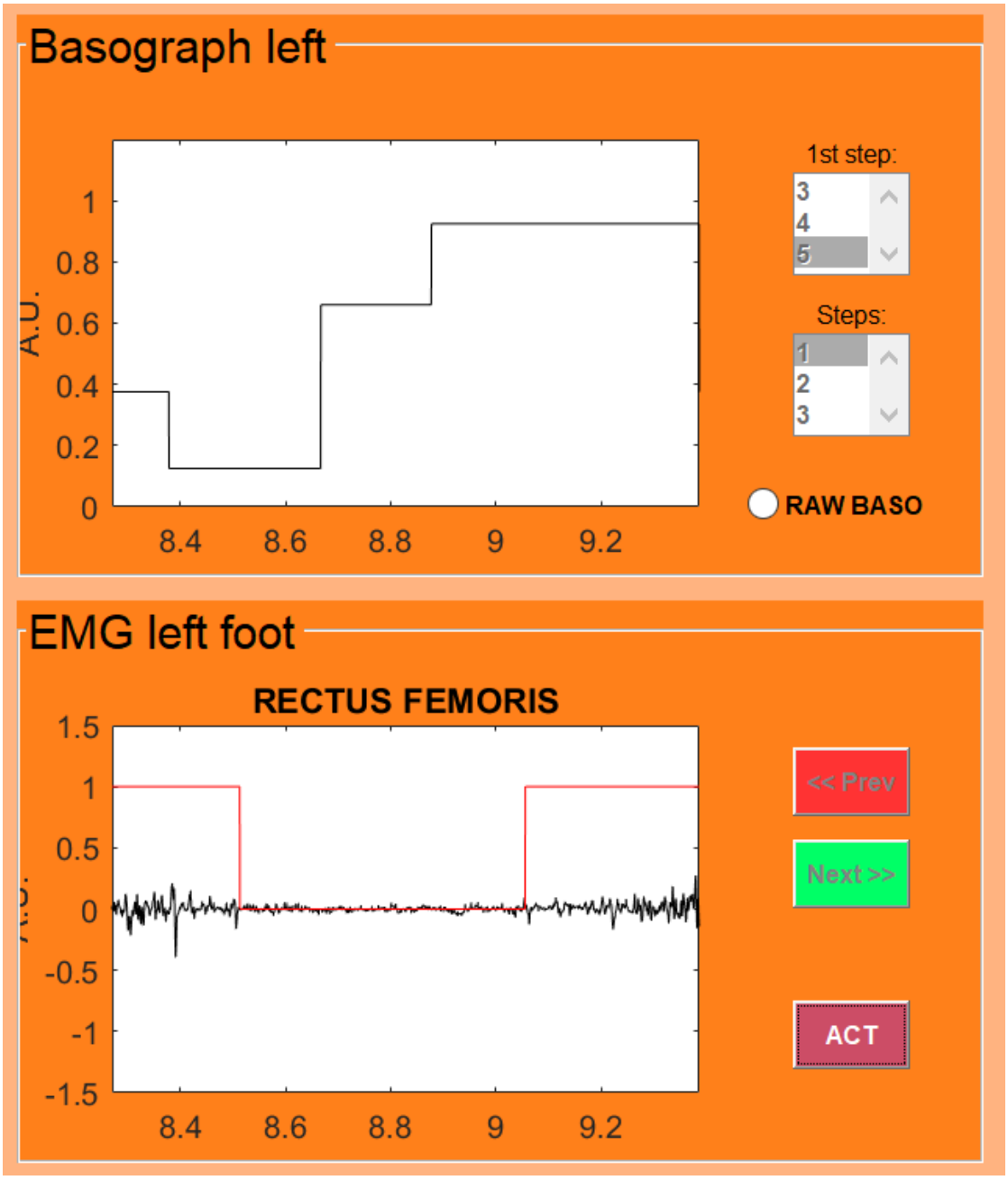

Figure 64: Rectus Femoris

Bibliography

[1] James B.Reswick, "How and when did the rehabilitation engineering center program come into being?", Journal of Rehabilitation Research & Development, Vol. 39 No. 6, 11-16, 2002.

[2] ®MATLAB, Creating Graphical User Interfaces

[3] Thomas E. Prieto et al., "Measure of Postural Steadiness: Differences Between Healthy Young and Elderly Adults", IEEE Transaction on Biomedical Engineering, Vol. 43, 1996.

[4] Jacquelin Perry, "GAIT ANALYSIS. Normal and Pathological Function",6900 Grove Road, Thorofare, NJ, SLACK Incorporated.

[5] Roy B. Davis III et al., "A gait analysis data collection and reduction technique", Human Movement Science, 10, 575-587, 1991.

[6] E. S. Grood, W. J. Suntay, "A Joint Coordinate System Description of Three Dimensional Motion: Application to the Knee", Journal of Biomechanical Engineering, Vol. 105, No. 2, 136-144, 1983.

[7] Stephane G. Mallat, "Multiresolution approximations and wavelet orthonormal bases of $L_2(\mathbb{R})$", Transaction of the American Mathematical Society, Vol. 315, 1, 1989.

[8] Carlo J. De Luca, "The Use of Surface Electromyography in Biomechanics", Journal of Applied Biomechanics, 13, 135-163, 1997.

[9] Andrea Merlo et al., "A Fast and Reliable Technique for Muscle Activity Detection From Surface EMG Signal",IEEE Transaction on Biomedical Engineering, Vol. 50, 2003.

[10] Paolo Bonato et al., "A Statistical Method for the Measurement of Muscle Activation Intervals from Surface Myoelectric Signal During Gait", IEEE Transaction on Biomedical Engineering, Vol. 45, 1998.

[11] Barr K. et al., "Surface Electromyography Does Not Accurately Reflect Rectus Femoris Activity During Gait: Impact of Speed and Crouch on Vasti-torectus Cross-talk." Gait Posture, 32:363-8, 2010.

[12] Nene A. et al.,"Is rectus femoris really part of the quadriceps? Assessment of the rectus femoris function during gait in able-bodied adults." Gait Posture, 10:1-13, 2004.

[13] Winter D. et al.,"Cross-talk in surface electromyography: theoretical and practical estimates." J Electromyogr Kinesiol 1994:415-26.